



#### ANNUAL REVIEWS **Further**

Click [here](#) to view this article's online features:

- Download figures as PPT slides
- Navigate linked references
- Download citations
- Explore related articles
- Search keywords

# Liquid Cell Transmission Electron Microscopy

Hong-Gang Liao<sup>1</sup> and Haimei Zheng<sup>1,2</sup>

<sup>1</sup>Materials Sciences Division, Lawrence Berkeley National Laboratory, Berkeley, California 94720; email: hmzheng@lbl.gov

<sup>2</sup>Department of Materials Science and Engineering, University of California, Berkeley, California 94720

Annu. Rev. Phys. Chem. 2016. 67:719–47

The *Annual Review of Physical Chemistry* is online at [physchem.annualreviews.org](http://physchem.annualreviews.org)

This article's doi:  
10.1146/annurev-physchem-040215-112501

Copyright © 2016 by Annual Reviews.  
All rights reserved

## Keywords

liquid cell TEM, environmental TEM, materials transformation, solid-liquid interfaces, biological imaging, electron beam effects

## Abstract

Liquid cell transmission electron microscopy (TEM) has attracted significant interest in recent years. With nanofabricated liquid cells, it has been possible to image through liquids using TEM with subnanometer resolution, and many previously unseen materials dynamics have been revealed. Liquid cell TEM has been applied to many areas of research, ranging from chemistry to physics, materials science, and biology. So far, topics of study include nanoparticle growth and assembly, electrochemical deposition and lithiation for batteries, tracking and manipulation of nanoparticles, catalysis, and imaging of biological materials. In this article, we first review the development of liquid cell TEM and then highlight progress in various areas of research. In the study of nanoparticle growth, the electron beam can serve both as the illumination source for imaging and as the input energy for reactions. However, many other research topics require the control of electron beam effects to minimize electron beam damage. We discuss efforts to understand electron beam–liquid matter interactions. Finally, we provide a perspective on future challenges and opportunities in liquid cell TEM.

## 1. INTRODUCTION

Transmission electron microscopy (TEM) is a powerful and indispensable tool for the characterization of materials, and it provides critical structural and chemical information for them. In recent years, significant advances have been made in electron microscopy. Concurrent with aberration-corrected (scanning) TEM, which has made atomic imaging and spectroscopy a routine process (1–3), it has now been possible to image materials in liquid (including gas) environments at the subnanometer or atomic scale. Imaging through liquids with TEM can be traced back to 1934, the beginning of electron microscopy, when Marton (4) imaged biological samples sandwiched between two thin aluminum foils. However, in the next several decades, there were limited activities (5–11) in this area, likely resulting from the technical challenges in isolating the liquid sample from the high-vacuum environment of an electron microscope: A conventional transmission electron microscope requires high vacuum ( $10^{-6}$  torr or higher) within the microscope column to minimize electron scattering other than that from the sample.

With technical advancements in liquid cell nanofabrication, imaging through liquids sandwiched between two ultrathin membranes with subnanometer resolution using TEM has only recently become possible. Liquid cell TEM is a fast-growing and fascinating area of research, which has drawn tremendous attention from various fields, ranging from materials science to chemistry, physics, and biology (12, 13). Many homemade liquid cells have been reported, and commercial liquid sample stages are available. Liquid cell TEM has been applied to the study of nanoparticle nucleation and growth (14–16); nanoparticle motion in solution (14–17); electrochemically driven reactions such as deposition, corrosion, and ion transportation (18–21); liquid nanodroplets and bubble formation (22, 23); biomineralization (24); organic materials (25, 26); and biological materials, such as proteins and whole cells in liquid water (27–29). **Figure 1** presents a statistic plot of published papers using the liquid cell TEM methodology over the years. It illustrates the drastic increase in publications in recent years (4–11, 14–19, 21, 23, 24, 26–28, 30–94). It is clear that liquid cell TEM plays an increasingly important role in a diverse set of scientific topics.

In this review, we first discuss the design and development of liquid cells and then review progress in different topics, including (*a*) the observation of nanoparticle formation, such as the mechanisms of nanoparticle growth and factors controlling nanoparticle morphology, including surfactants, neighboring particles, and precursor concentration; (*b*) tracking and manipulation of nanoparticles in a liquid cell; (*c*) the study of electrode-electrolyte interfaces using an electric biasing liquid cell; and (*d*) bioscience applications of liquid cell TEM. We also summarize the current understanding of electron beam–liquid matter interactions and our perspective on controlling electron beam effects. Finally, we provide an outlook of the future developments and applications of liquid cell TEM.

## 2. LIQUID CELL DEVELOPMENT

### 2.1. Design and Fabrication of Liquid Cells

Most liquids, including water and other organic solvents, have a high vapor pressure; thus, they are incompatible with the high-vacuum environment of a transmission electron microscope. A sealed liquid cell is required to separate water and other high-vapor pressure liquids from the vacuum environment. At the same time, the imaging window needs to be thin enough to allow the electron beam to go through and sufficiently strong to sustain the high vacuum. These general requirements and the concept of using a window-confined cell in TEM were discussed even in

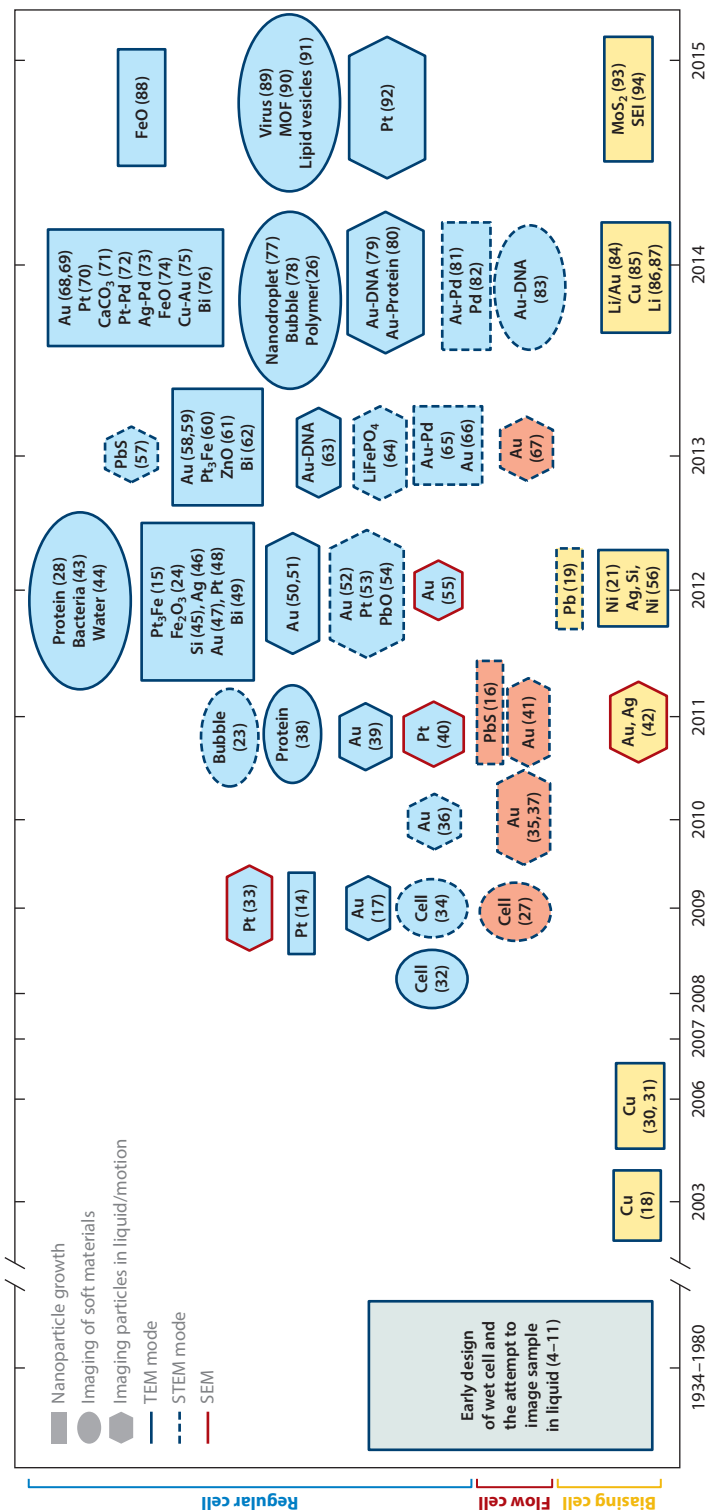


**Figure 1**

A statistic plot of publications related to liquid cell electron microscopy since 1934. Abbreviations: MOF, metal organic framework; SEI, solid electrolyte interphase; SEM, scanning electron microscopy; STEM, scanning transmission electron microscopy; TEM, transmission electron microscopy.

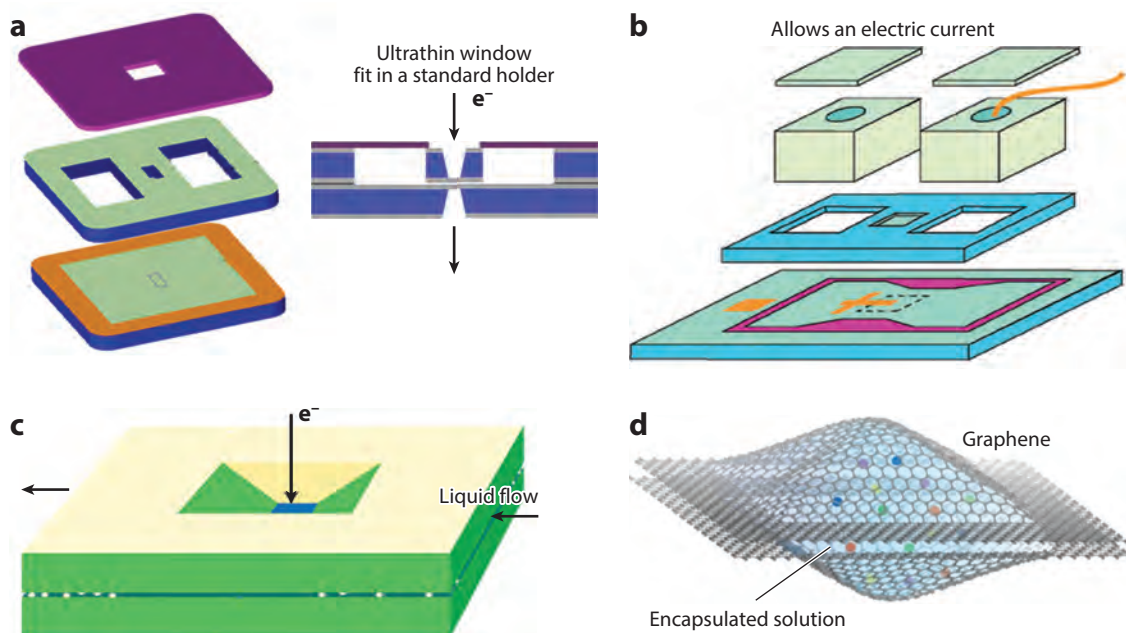


**Figure 2**

Different types of liquid cells reported in recent years. (a) A self-contained liquid cell with an ultrathin SiN<sub>x</sub> membrane window. It can fit in a standard transmission electron microscopy sample holder. Panel a adapted from Reference 14 with permission. (b) An original electrochemical liquid cell with patterned electrodes inside the cell. Panel b adapted from Reference 18 with permission. (c) A flow cell allowing liquids to flow between two chips. Panel c adapted from Reference 27 with permission. (d) A graphene cell. Panel d adapted from Reference 96 with permission.

the earliest days of electron microscopy (reviewed in 95). From the early attempt of imaging wet samples using sandwiched thin aluminum foils (4) to the current functional thin SiN<sub>x</sub>/Si liquid cells (**Figure 2a–c**) and graphene liquid cells (**Figure 2d**), there was a several-decades gap, during which the standard TEM protocol of imaging dry samples *ex situ* by periodically stopping the reaction was applied. However, the dynamic processes of materials during reactions cannot be obtained using such an *ex situ* practice.

In 2003, Williamson et al. (18) reported the development of a liquid cell for TEM using silicon wafers with an electron transparent silicon nitride membrane window. Gold electrodes were deposited on the bottom chip, and it was glued together with the top chip with a glass spacer in between, forming an electrochemical liquid cell. Additional containers for liquid electrolyte were assembled in the electrochemical cell for electric biasing experiments (**Figure 2b**). The electrochemical deposition of copper clusters on the gold electrode was studied *in situ*. Because the electron beam has to penetrate a thick layer of mass (e.g., two silicon nitride membranes, each 100 nm, a 50-nm gold electrode, and over a 1-μm-thick liquid layer), limited resolution was achieved at that time (30, 31).

To study colloidal nanocrystal growth under TEM, Zheng et al. (14) reported in 2009 the development of self-contained liquid cells and achieved 1-nm resolution. Much thinner SiN<sub>x</sub> membranes (25 nm) were used for the liquid cell window, and a liquid layer of 100 nm was obtained using a sticky metal layer of indium as the spacer between the bottom and top chips. To make sure the thin membrane could survive the high vacuum, they used a much smaller rectangular window

of about a few micrometers by 50  $\mu\text{m}$  instead of the previous  $100 \times 100\text{-}\mu\text{m}$  window. Such thin silicon nitride liquid cells enabled the study of single platinum nanoparticle growth trajectories, and the unique growth mechanisms of colloidal nanoparticles through monomer attachment or coalesce were revealed (14). This work attracted much attention in the field of colloidal chemistry, and many studies on nanoparticle growth using liquid cell TEM have emerged (15, 60, 62, 70).

It is also possible to flow liquids between two silicon nitride membranes of a liquid cell using external tubing and a syringe pump (37). In 2009, de Jonge et al. (27) described the use of a flow cell to image whole cells in liquids (**Figure 2c**). The liquid flow capability is appealing to researchers interested in reactions involving mixing solvents instantaneously or injecting reactant agents into another type of liquid. Critical issues still need to be addressed, such as sample drift introduced by liquid flow, membrane rupture, and potential contamination. In many cases, a still liquid environment similar to that in a self-contained liquid cell is maintained during imaging.

In 2012, a graphene liquid cell for high-resolution imaging during platinum nanocrystal growth was reported (96). Small droplets of liquids are enclosed between two graphene sheets to fabricate a graphene liquid cell. As graphene is impermeable to liquids, and it is the thinnest material, the graphene liquid cell allows imaging with unprecedented high resolution. The development represents a significant advancement despite limitations on the kinds of experiments that can be performed using the cell.

Compared to graphene cells, silicon nitride liquid cells are still highly attractive as  $\text{SiN}_x$  is mechanically strong and relatively inert, and has low imaging contrast. Most importantly, an  $\text{SiN}_x/\text{Si}$  liquid cell provides an excellent developing platform for functional measurements, such as allowing experiments under an electric bias (18), heating (49, 62), and cooling (97). However, there are also issues associated with silicon nitride liquid cells. For instance, the pressure difference across the membranes can cause them to bow outward, inducing a thicker liquid layer. Efforts have been made to accurately measure the thickness of the imaging window and to limit the membrane bowing. Electron energy loss spectroscopy (EELS) has been used to estimate the window thickness (46, 57, 66, 95), and the results demonstrate that bowing can increase the liquid thickness by a factor of three in a typical liquid cell with a  $50 \times 50\text{-}\mu\text{m}$   $\text{SiN}_x$  membrane window (54). There are ways to minimize window bowing, such as thinning small areas within a thicker membrane to generate a patterned window (98) and reducing the total size of the membrane window (70).

In general, in a liquid cell experiment, the liquid solution is loaded into the cell, and the cell is placed on a conventional TEM sample holder or a commercial liquid stage. Then the liquid cell is tested to avoid leakage before it is loaded into the microscope. For studies of nanoparticle growth, the electron beam can be the energy source to drive the reaction. However, for studies of an electrochemical process or when imaging many other liquid samples, electron beam effects need to be controlled. In general, for real-world reactions, it is critical to understand electron beam–matter interactions and implement low-dose imaging techniques. Details on electron beam effects are discussed in Section 7.

In parallel to the development of a sealed liquid cell for liquid samples, an open cell with droplets of low-pressure liquids, particularly ionic liquids, has been reported. This open cell concept was initiated by Wang et al. (99) and Huang et al. (100) as the cell was developed to study battery electrode materials during lithiation and delithiation. We briefly discuss their work in Section 5.2. However, in this article, we focus on work using sealed liquid cells.

## 2.2. Information Available from Liquid Cell Transmission Electron Microscopy

With the ability to image through liquids with subnanometer resolution, liquid cell TEM has enabled, for example, the tracking of single nanoparticle growth trajectories, dynamic nanoparticle

movement in liquids, electrochemical deposition and lithiation of electrode materials, and the imaging of biological materials in liquid water. By combining other imaging and spectroscopy techniques, such as scanning transmission electron microscopy (STEM), energy dispersive X-ray spectroscopy, selected area electron diffraction, and EELS, researchers have provided rich information on the dynamic processes of materials (50, 64, 65).

For studies of materials transformations, there are many other *in situ* approaches, such as *in situ* optical spectroscopy (101), X-ray spectroscopic methods (102–106), atomic force microscopy (AFM), and scanning tunneling microscopy (STM) (107–109). Oezaslan et al. (110) reported *in situ* measurements of bimetallic platinum-copper alloy nanoparticles using high-temperature X-ray diffraction. Polte et al. (104) investigated the growth of nanoparticles from an average radius of 0.8 nm to 2 nm by time-resolved small-angle X-ray scattering with millisecond time resolution. Simm et al. (108) used *in situ* AFM to study the growth of cobalt nuclei on a boron-doped diamond electrode under potentiostatic control. The growth of the nuclei as a function of time was monitored under different deposition potentials. With these *in situ* methods, critical information on nucleation and growth has been achieved. However, these methods also have their limitations. For example, *in situ* spectroscopy methods lack the ability of direct visualization; AFM and STM techniques can be used only to image samples on a substrate; and the temporal resolution is also limited.

Liquid cell TEM has unique advantages in allowing the direct observation of the dynamics of materials transformation in liquids with high spatial and temporal resolution. It is also applicable to imaging of various organic materials and biological materials in a liquid phase. The major criticisms of the technique come from the damage caused by electron beam radiation and challenges in controlling the local temperature and reactant mixing, for example, during reactions. We discuss these issues in Section 7.

### 3. NANOPARTICLE GROWTH OBSERVED IN A LIQUID CELL

#### 3.1. Tracking Single Nanoparticle Growth Trajectories

Although colloidal nanoparticle synthesis has advanced significantly over the past 20 years, and nanoparticles with different size, shape, and architectures have been achieved, the prevalent approach to developing new nanomaterials is a trial-and-error process based on the resulting nanostructures. This is fundamentally limited in that the growth processes can be inferred only from the final synthetic structure. Such postmortem analysis cannot provide enough information on the synthesis process. Tracking single nanoparticle growth trajectories using a liquid cell provides an opportunity to develop a fundamental understanding of nanoparticle evolution and to elucidate nanoparticle growth mechanisms.

According to the classical theory of Ostwald ripening, nanoparticle growth proceeds by monomer attachment to an existing nucleus. It was assumed that growth by nanoparticle coalescence should be avoided to achieve monodisperse nanoparticles. By direct observation of platinum nanoparticle growth in a liquid cell, Zheng et al. (14) discovered that two types of growth, either by monomer attachment or by coalescence, lead to the same particle size. As shown in **Figure 3a**, the coalesced nanoparticles can eventually become a spherical nanoparticle, similar to that created by monomer attachment. Growth by nanoparticle attachment has also been demonstrated in Pt<sub>3</sub>Fe nanowire formation. Liao et al. (15) observed the growth of Pt<sub>3</sub>Fe nanowires by nanoparticles attached end to end (**Figure 3b**). Such nanoparticle chain formation was attributed to the dipolar interaction between nanoparticles. Using a graphene liquid cell, Yuk et al. (96) studied platinum nanoparticle growth with superior resolution. They found that coalescence is a site-selective,

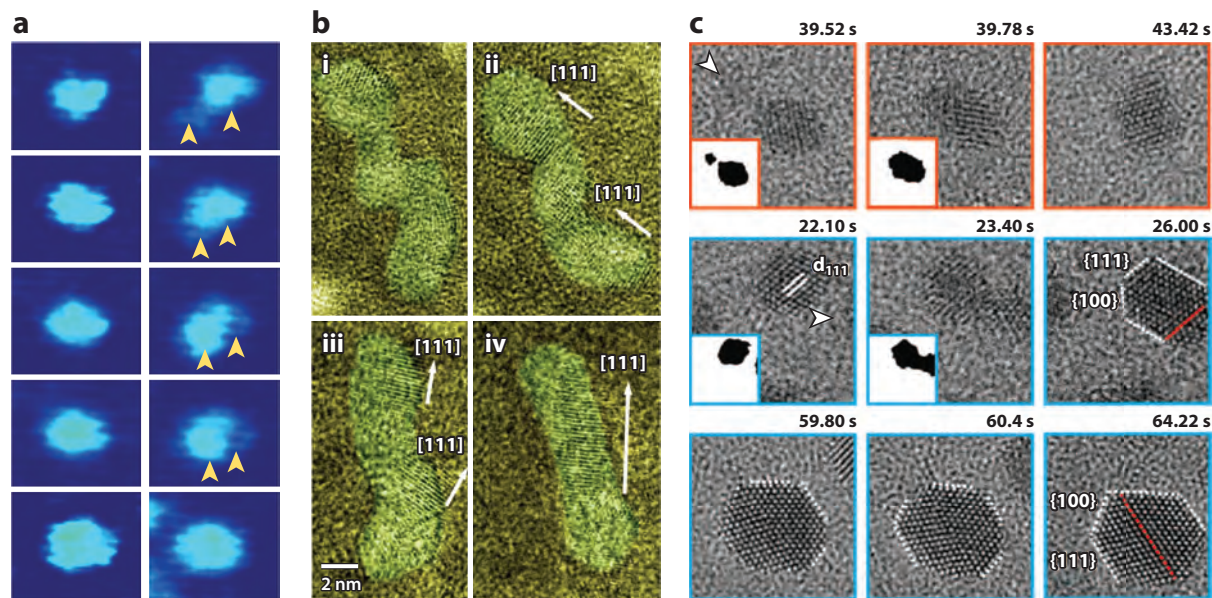


**Figure 3**

Single nanoparticle growth trajectories studied using a liquid cell. (a) Sequential images showing platinum nanoparticle growth either by monomer attachment or by nanoparticle coalescence, leading to the same particle size. Yellow arrowheads represent the attaching of nanoparticles. Panel *a* adapted from Reference 14 with permission. (b) Sequential high-resolution transmission electron microscopy images showing both the crystal orientation and shape changes during the straightening of a twisted nanoparticle chain. Panel *b* adapted from Reference 15 with permission. (c) Platinum nanocrystal growth via coalescence and crystal-structure evolution observed with atomic resolution in a graphene liquid cell. White arrowheads denote incoming small nanocrystals, red dotted lines indicate the twin boundary, and the red and blue box outlines represent different sets of data. Panel *c* adapted from Reference 96 with permission.

specific facet, with the lowest surface energy or lowest ligand coverage ( $\{111\}$  for fcc) preferred during nanoparticle attachment. With atomic rearrangement after coalescence, a single crystal or a twinned nanoparticle is formed (Figure 3c).

Along with the above studies, there have been many reports on nanoparticle growth by monomer attachment or the coalescence of nanoparticles (including oriented attachment). We highlight a few selected from the literature below. These liquid cell TEM studies of nanoparticle growth provide useful information for our understanding of growth mechanisms of the selected nanoparticle system.

Liu et al. (61) reported ZnO nanoparticle precipitation for which they found that both Ostwald ripening and coalescence are the early stage growth mechanisms; however, nanoparticle aggregated growth is dominant at the later stage. Zhu et al. (82) showed that the growth of palladium dendrites can be achieved after nucleation of a cluster with the beam probe.

Woehl et al. (46) studied the relationship between the nanoparticle growth rate and electron beam dose rate. They reported that a low beam current facilitates reaction-limited growth, leading to faceted nanocrystals, whereas a higher beam current promotes diffusion-limited growth, introducing spherical nanocrystals. It was also demonstrated that lead sulfide nanoparticles grow by selectively decomposing a chemical precursor from a multicomponent solution (16).

Niu et al. (76) found that symmetric coalescence with two equal-size nanoparticles and asymmetric coalescence with two or more unequal-size nanoparticles are possible during the growth of bismuth nanoparticles. Both surface diffusion and grain boundary diffusion are mass transport

mechanisms during the relaxation period after coalescence. The relaxation time increases with the particle size. There is competition between coalescence and the collision time; the collision time is determined by factors such as nanoparticle concentration and the speed of nanoparticle movement, whereas the electron beam influences coalescence. Aabdin et al. (111) studied gold nanocrystal bonding in solution and found two pathways: (a) Coherent, defect-free bonding occurs when two nanocrystals attach with their lattices aligned within a critical angle, and (b) beyond this critical angle, defects form at the interfaces where the nanocrystals merge.

Interaction between nanoparticles is an important factor during nanoparticle growth, which may involve, for example, van der Waals forces, hydrophobic interaction, magnetic force, and charge interaction. Liu et al. (59) observed CTA-gold nanoparticle self-assembly to form nanoparticle chains. Anisotropic attractive interactions and size-dependent segregation have been reported, in agreement with Liao et al.'s (15) findings on the electrostatic dipolar interaction between Pt<sub>3</sub>Fe nanoparticles.

Woehl et al. (112) reported that the growth of silver nanoparticles is length-scale dependent, in which individual nanoparticles grow by monomer attachment and the ensemble large-scale growth is dominated by aggregation. Direct observations of aggregation revealed that growth follows a Smoluchowski model, and both the mean growth rate and particle size distribution were captured.

Li et al. (24) observed oriented attachment during iron oxide nanoparticle growth. Nanoparticles underwent continuous rotation and interaction before they found the perfect lattice match with the same orientation. Measured translational and rotational accelerations demonstrate that strong, highly direction-specific interactions drive crystal growth via oriented attachment.

### 3.2. Nanoparticle Shape Evolution

The shape of nanocrystals strongly influences their performance in catalysis, sensing, and many other surface-enhanced applications (113, 114). Nanoparticles with various shapes have been achieved, such as nanodots, one-dimensional (1D) nanowires and nanorods, faceted nanoparticles, and multipod nanostructures. However, the crystallization process is complex, involving the arrangement of thousands of atoms or molecules near the surface, and it is further complicated by interactions between atoms and influences from the surroundings. With environmental modifications, such as temperature, precursor, and surfactants, it is possible to control the reaction and growth to create nanocrystals with different shapes and structures. However, the shape-controlled mechanisms during colloidal synthesis are often not well understood or characterized. Liquid cell TEM has been proven to be a unique and effective method to study nanoparticle growth and to unravel the role of different factors in controlling the structure and morphology of nanoparticles.

Wulff construction (115, 116) has been used to predict the equilibrium shape of nanocrystals. It states that the length of a normal vector drawn from the crystal center to an external surface is proportional to the surface free energy. It is widely accepted that in nanocrystal growth, the high-energy facets grow at a higher rate than the low-energy facets; therefore, the fast-growing facets will eventually disappear, resulting in a nanocrystal terminated with low-energy facets (117, 118). It is assumed that the commonly used surfactants modify the energy of specific facets through preferential adsorption, influencing the relative growth rate of different facets and thus the shape of a nanocrystal (119, 120). However, the evolution of nanoparticle morphology is largely unknown, and the shape control mechanisms of nanocrystals need to be further explored. Recently, Liao et al. (70) imaged platinum nanocube growth using liquid cell TEM, showing that the surface energy minimization rules break down at the nanoscale. As shown in **Figure 4**, the growth rates of all low-index facets, {100}, {110}, and {111}, are similar until the {100} facets stop growing.

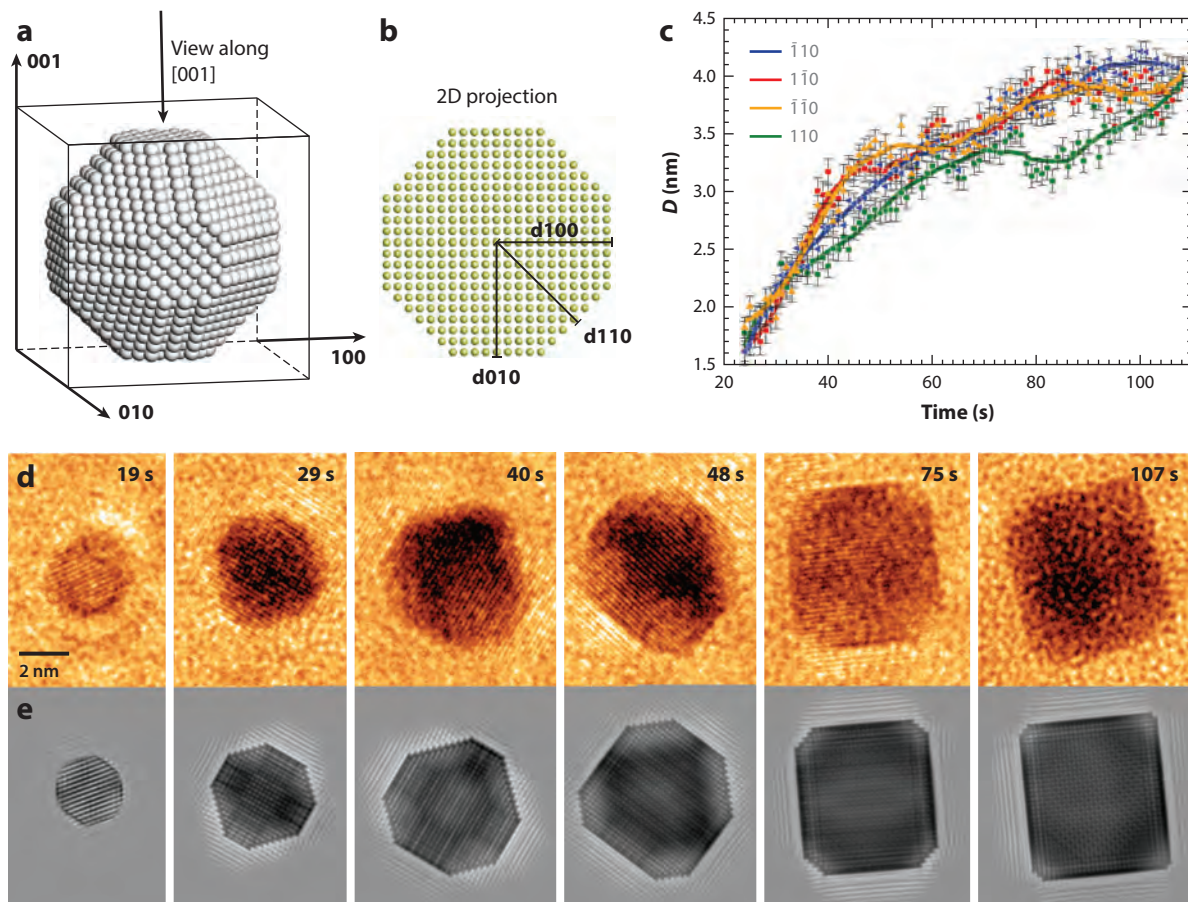


**Figure 4**

(a) The facet development of a platinum nanocube viewed along the  $[0\bar{1}1]$  axis. (b) The atomic model of a truncated platinum nanocube and its projection along the  $[0\bar{1}1]$  view zone axis. The distance from the crystal center to each of the  $(100)$ ,  $(011)$ , and  $(111)$  facets is highlighted. (c) The measured average distance from the crystal center to each facet as a function of time. (d) Sequential images showing the growth of the platinum nanocube. (e) Simulated transmission electron microscopy images of the platinum nanoparticle in panel d. Figure adapted from Reference 70 with permission.

The  $\{110\}$  facets continue to grow until they reach a limit, at which point they form an edge of a nanocube. The continued growth of  $\{111\}$  facets fills the corners of the cube. In combination with density functional theory calculation, such direct observation of atomic facet development in platinum nanocube growth reveals the selective facet-arrested shape control mechanisms. This work is an excellent example demonstrating that liquid cell TEM is highly useful in revealing hidden mechanisms of nanocrystal growth with high spatial and temporal resolution.

Besides modifying the growth rate of certain facets, surfactants can drastically influence the morphology of the final nanoparticles, inhibit nanoparticle aggregation, and prevent coalescence. Zheng et al. (14) found that, by decreasing surfactant within platinum nanoparticle growth, foil and dendrites could be obtained. Liao et al. (60) showed that it is essential to control oleylamine concentration to achieve platinum-iron nanoparticles with a desired shape. For instance, 20% oleylamine in the precursor solution led to an unstable nanoparticle chain that eventually broke into

nanoparticles; 30% oleylamine resulted in stable nanowires in the solution; and 50% oleylamine prevented nanoparticles from merging together, and the shapes were influenced by neighboring particles (**Supplemental Figure 1**; follow the **Supplemental Material link** from the Annual Reviews home page at <http://www.annualreviews.org>).

Growth with temperature control in a liquid cell has also been achieved. Xin & Zheng (49) reported the growth of bismuth nanoparticles in a TEM liquid cell at an elevated temperature using a commercial heating sample stage. The oscillatory growth dynamics of bismuth nanoparticles were observed when the liquid cell was heated to 180°C. Both individual and pairwise growth oscillations and collective fluctuations at global length scales were achieved. They also demonstrated that a depletion zone is present around a particle. This study suggests the possibility of counteracting the energetically favorable Ostwald ripening process to prevent nanoparticle coarsening, which is highly beneficial in the design of many industrial reactions, such as heterogeneous nanoparticle catalysis.

Solvent is another critical factor for morphology control. Among the three commonly used solvents in liquid cell TEM experiments (water, organic solvent, and ionic liquid), aqueous solution is most challenging to handle. Interactions between water molecules and the electron beam result in the ionization of water, from which different radicals can be generated. Organic solvent has also been widely used. Zheng's (14, 15, 60, 62, 70, 76, 121) research group used the organic solvent of pentadecane, dichlorobenzene, benzene ether for the growth of platinum nanospheres and nanocubes, Pt<sub>3</sub>Fe nanowires, bismuth nanospheres, etc. Yuk et al. (96) used a mixture of o-dichlorobenzene and oleylamine (9:1 in volume ratio) for platinum nanoparticle growth in a graphene liquid cell. As for ionic liquid, it can be used directly in the vacuum environment without evaporation issues or charging effects. For instance, using C<sub>9</sub>H<sub>13</sub>BrN<sub>2</sub> supported on a hole in a TEM grid by surface tension, Kimura et al. (122) studied NaClO<sub>3</sub> nucleation. The simultaneous formation and dissolution of prenucleation clusters and the formation of different phases were observed.

### 3.3. Growth of Heterostructured Nanoparticles

There have been many liquid cell TEM studies on the heterogeneous growth of nanoparticles using nanoparticle seeds. Nanostructures with complex shapes and architectures have also been achieved. Here we review some of these studies, which show diverse discoveries on different systems.

Using liquid cells, Sutter and colleagues (65, 73) investigated the heterogeneous growth of palladium on gold particle seeds. By using nanoparticle seeds in a precursor solution and taking advantage of radiolysis or galvanic replacement, they grew gold-palladium core-shell nanoparticles. They found that the size and shape of the gold seeds determined the morphology of the palladium shells. For small gold particles (5 nm), continuous and uniform shells were achieved by palladium monomer incorporation from the solution. In large particles (15 and 30 nm), nonuniform growth caused the palladium shell thickness to vary, and the slower depletion of palladium ions in the solution promoted competing growth process. They proposed that the hydrated electrons induced by the electron beam can reduce the chloropalladate complexes and influence the heterogeneous growth process. Heterogeneous growth is limited by the diffusion of hydrated electrons in the solution (65) (**Figure 5a**). Further analysis demonstrated that the as-grown palladium shell contains palladium-chloro complexes and that the redox reaction is first order with respect to the concentration of hydrated electrons. Sutter et al. (73) also investigated galvanic replacement reactions between a silver nanoparticle and aqueous palladium salt solution by using liquid cell TEM, transforming the silver particles into hollow silver-palladium nanostructures.

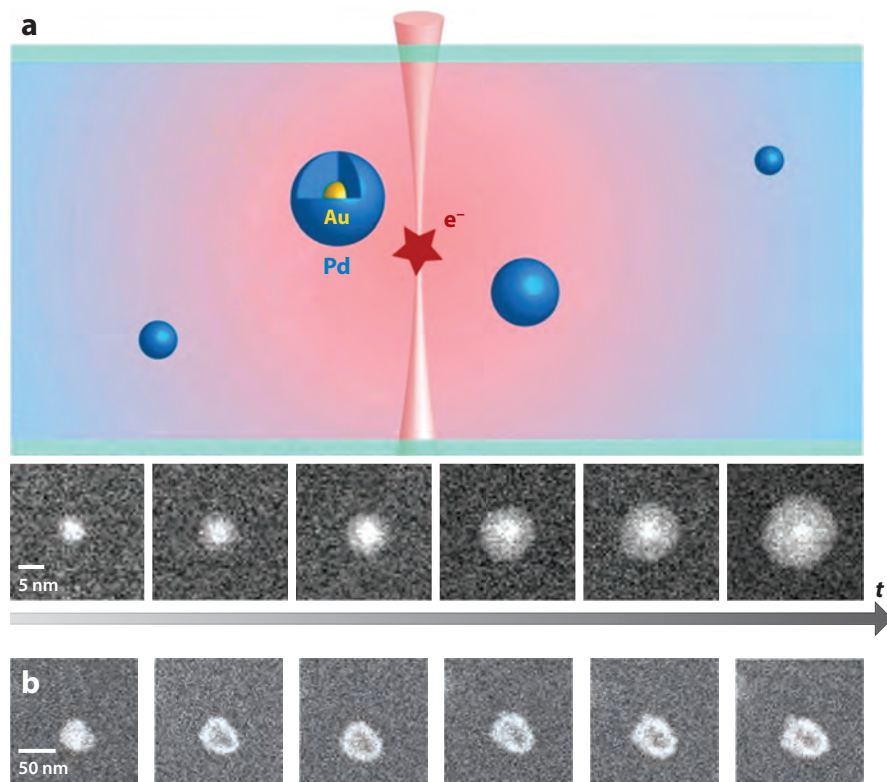


**Figure 5**

(a) Heterogeneous growth of palladium on gold seeds, forming a gold-palladium core-shell nanostructure. Panel *a* adapted from Reference 65 with permission. (b) Evolution of a silver particle in aqueous  $\text{PdCl}_2$  solution. Panel *b* adapted from Reference 73 with permission.

By comparison with ex situ experiments, the authors concluded that the electron beam strongly affects the galvanic-type process in the liquid cell (**Figure 5b**).

Wu et al. (123) recently studied the nucleation and growth of gold on platinum icosahedral nanoparticles. Quantitative analysis of growth kinetics was carried out based on real-time TEM observation. They showed that the growth process involves (a) the deposition of gold on corner sites of platinum icosahedral nanoparticles, (b) the diffusion of gold from corners to terraces and edges, and (c) the subsequent layer-by-layer growth of gold on gold surfaces to form platinum-gold core-shell nanoparticles. The in situ TEM results indicate that the diffusion of gold from corner islands to terraces and edges is kinetically controlled, as evidenced by measurements of diffusion coefficients for these growth processes.

Kraus & de Jonge (58) observed the growth of gold dendrites on gold nanoparticle seeds. They concluded that there is no correlation between the local seed morphology and the emerging dendrite morphology and that the dendrite growth is limited by diffusion. Zhang and colleagues (82) investigated the growth of 2D palladium dendrites in a liquid cell. They proposed that diffusion-limited aggregation and atomic deposition are responsible for the dendrite growth. Lewis et al. (75) investigated dynamic liquid-phase synthesis of core-shell nanostructures, in which they conducted

elemental mapping of nanostructures in solution to the compositional distribution for multiple elements within the resulting materials.

De Clercq et al. (72) reported the growth of platinum-palladium nanoparticles in a graphene oxide liquid cell. They found that the growth dynamics follow a power law with a growth exponent of 0.5, in agreement with the LSW (Lifshitz-Slyozov-Wagner) model in cases in which growth is limited by surface reaction. They proposed that surface reaction-limited growth mainly results from graphene oxide substrate effects, which pin the as-grown cluster and limit the coalescence of particles.

Liao et al. (68) studied the growth mechanism of fivefold twinned gold nanocrystals by imaging particle growth in an ionic liquid in situ. They identified the fivefold twinned nanocrystal growth pathways and proposed that nanoparticle sintering plays an important role in multi-twinned nanocrystal formation. Zhu et al. (82) studied the growth of 2D palladium dendritic nanostructures using in situ liquid cell TEM. Detailed in situ and ex situ high-resolution scanning TEM (S/TEM) characterization and fractal dimension analyses revealed that diffusion-limited aggregation and direct atomic deposition are responsible for the growth of palladium dendritic nanostructures.

### 3.4. Synthesis with a Template

Parent et al. (124) directly observed synthesis in a highly viscous lyotropic liquid crystal template at the nanoscale using fluid stage STEM. The nanoparticles nucleated and grew into 5-nm nanoparticles, at which point growth continued through the formation of connections with other nanoparticles around the micelles. Upon reaching a critical size ( $>10\text{--}15\text{ nm}$ ), the clusters became highly mobile in the template, displacing and trapping micelles within the growing structure to form spherical, porous nanoparticles. The final products matched those synthesized ex situ in the lab. This ability to directly observe synthesis at the nanoscale in rheological fluids, such as concentrated aqueous surfactants, provides an understanding of fundamental steps of nanomaterial growth. Parent et al. (125) also observed the growth of mesoporous palladium in a solvated block copolymer template under various synthesis conditions. The electron beam induced the nucleation of small particles in the aqueous phase around the micelles. The small particles flocculated and grew into denser structures that surrounded the micelles, forming an ordered mesoporous structure.

### 3.5. Etching and Corrosion

Oxidative etching prevails in the synthesis of nanocrystals. Jiang et al. (126) reported an in situ study of the oxidative etching of palladium cubic nanocrystals by liquid cell scanning TEM (**Supplemental Figure 2**). The etching was realized with oxidative radiation reactants from electron-water interaction in the presence of  $\text{Br}^-$  ions. Dissolution dynamics of monodispersed and aggregated nanocrystals were investigated and compared. Analyses on the dissolution kinetics of nanocrystals and the diffusion kinetics of the dissolved agents were carried out. The results provide quantitative information on the oxidative etching reaction.

The corrosion of metals or alloys is another branch of study that liquid cell TEM may impact. Developing an understanding of localized corrosion mechanisms remains a great challenge. Chee et al. (127) studied the localized corrosion of copper and aluminum thin films exposed to aqueous NaCl solutions using liquid cell TEM. They show the initiation of corrosion by applying an electric potential to an aluminum film, and the compositional changes can be used to modify corrosion susceptibility.

#### Supplemental Material

## 4. TRACKING AND MANIPULATION OF NANOPARTICLE MOVEMENT IN A LIQUID CELL

### 4.1. Tracking Single-Particle Motion

Nanoparticles move in solution. The motion of nanoparticles in a liquid cell may come from, for example, Brownian motion, chemical reaction-induced local environmental changes, liquid flow, and electron beam effects. It is important to develop an understanding of the physics and origin of nanoparticle motion. As the thickness of solution in a liquid cell approaches the nanometer scale, several factors influence particle motion, including solvent surface fluctuations and vapor-liquid or liquid-substrate interfaces, as well as intrinsic differences in relaxation and transport properties in an ultrathin liquid film compared to its bulk. In an ultrathin liquid film, the viscosity can be much higher than the bulk liquid, and the interaction between the solvent molecules and substrate surface can impact nanoparticle diffusion. The diffusion of nanoparticles in such thin liquid films is largely beyond the predictive capabilities of current theoretical computation.

So far, there have been many reports on nanoparticle motion imaged by liquid cell TEM in which both self-contained liquid cells (14) and flow cells (37, 50) were used. By taking advantage of the high spatial resolution of TEM, Zheng et al. (17) observed the microscopic details of nanoparticle motion during fluid evaporation. Tracking real-time diffusion of both spherical (5–15 nm) and rod-shaped ( $5 \times 10$  nm) gold nanocrystals in a thin film of water–15% glycerol revealed complex nanoparticle movements, such as rolling motions coupled to large-step movements and macroscopic violations of the Stokes-Einstein relation for diffusion. As drying patches form during the final stages of evaporation, particle motion is dominated by the nearby retracting liquid front.

Chen et al. (63) reported 3D motion of DNA-gold nanoconjugates in a graphene liquid cell (**Figure 6a**). The quantitative analysis of real-time nanocrystal trajectories shows that double-stranded DNA dictates the motion of linked nanocrystals throughout the imaging time of minutes. This sustained connecting ability of double-stranded DNA enabled continuous imaging under TEM, which is rarely achieved.

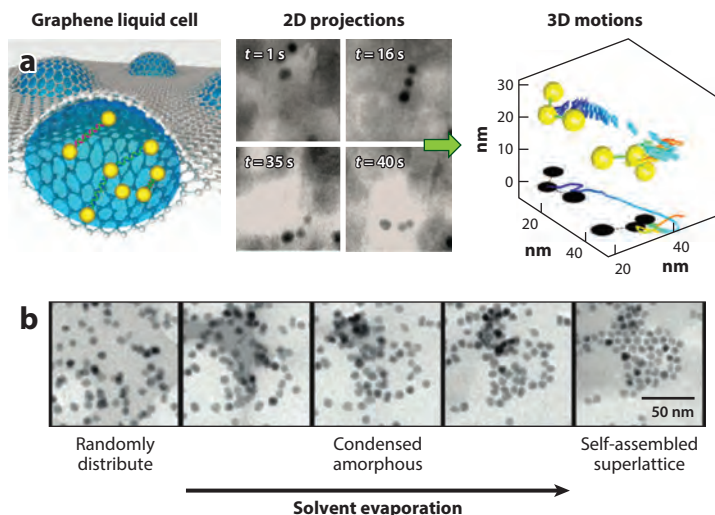


**Figure 6**

(a) Imaging of 3D motion of DNA-gold nanoconjugates (63). (b) In situ observation of superlattice formation by liquid cell transmission electron microscopy. Figure adapted from Reference 48 with permission.

Using STEM, de Jonge et al. (35) were able to image gold nanoparticles in water with a thickness of several micrometers. White et al. (23) studied charged platinum nanoparticle dynamics in water. Furthermore, Mueller et al. (67) captured the motion of gold nanorods in a flow cell.

Nanoparticle motion can also be utilized for the 3D reconstruction of nanoparticles. Park et al. (92) presented a hybrid method for reconstructing 3D structures of individual nanoparticles in solution. They used a graphene cell to image free rotating platinum nanoparticles in solution and derived the 3D structure at the near-atomic scale from images of individual nanoparticles, providing a way to understand the structure and stability of defects at the nanoscale (**Figure 7**).

## 4.2. Observation of Nanoparticle Assembly

The self-assembly of nanoparticles has attracted great attention. Assembled nanoparticles may show collective properties from different types of materials, with each kind of nanoparticles showing homogeneous and tunable properties with respect to their composition, size, and shape (128, 129). Nanoparticle assemblies are often formed empirically. An understanding of the fundamental mechanisms of assembly formation may help guide the creation of large-scale nanoparticle arrays suitable for effective device architectures. Liquid cell TEM provides a direct imaging platform to visualize the self-assembly of nanoscale objects. Although diffusion in a liquid nanofilm near the surface can vary from the real bulk liquid, nanoparticle self-assembly observed in a liquid cell provides useful information on the interaction between nanoparticles.

Park et al. (48) reported that an ordered nanoparticle superlattice can be formed from randomly distributed nanoparticles (**Figure 6b**), with both capillary forces and local solvent fluctuations by electron beam-induced local evaporation playing a role in the assembly process. Liao et al. (60) reported that nanoparticles can be self-assembled into a chain, ring, and 2D film during nanoparticle growth. Grogan et al. (39) observed the aggregation of gold nanoparticles using a custom-made liquid cell. The kinetics of movement and fractal dimension of the aggregates are consistent with 3D cluster-cluster diffusion-limited aggregation. Liu et al. (59) reported that a high-energy electron beam can induce the self-assembly of gold nanoparticles coated with positively charged CTA<sup>+</sup> and negatively charged citrate (CI<sup>-</sup>) ions in solution. Because of the different surface charges, gold nanoparticles behaved differently as they were illuminated with the electron beam. The self-assembly of positively charged gold nanoparticles into a chain was observed when the electron beam intensity exceeded a threshold of 5 pA/cm<sup>2</sup>, whereas negatively charged particles remained stationary regardless of the electron beam intensity.

## 4.3. Manipulation of Nanoparticles with Electron Beam

A highly focused electron beam can be used to manipulate nanoparticle movement (i.e., electron tweezers) and to probe the interaction forces between nanoparticles while observing dynamic nanoparticle motion. Oleshko & Howe (130) reported early work on electron tweezers. They showed that 20–300-nm solid aluminum particles inside a molten aluminum-silicon eutectic alloy can be trapped and steered using a focused electron beam inside a transmission electron microscope. Batson et al. (131, 132) reported the use of a swift electron beam in STEM to control the position of gold nanoparticles on an amorphous carbon film.

Zheng and colleagues (51, 133) reported the electron beam manipulation of gold nanoparticle movement in a liquid cell using TEM (**Supplemental Figure 3**). The degree of flexibility in nanoparticle manipulation was remarkable. Gold nanoparticles were trapped inside the beam, and their global movements followed the movement of the beam. The unique discovery in this work is that the trapping force of the electron beam was directly measured by the probability distribution of the gold nanoparticles, and it was calculated to be approximately 1 pN. Using an electron

### Supplemental Material

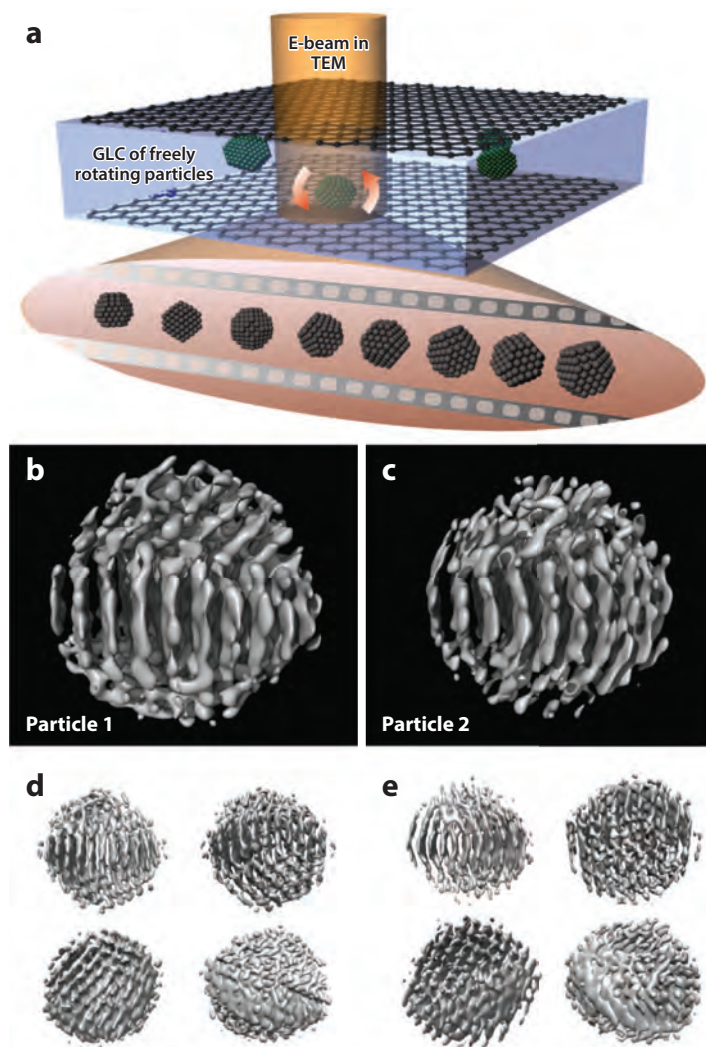


**Figure 7**

Illustration of in situ TEM imaging of platinum nanocrystals freely rotating in a graphene liquid cell and 3D electron microscopy density maps calculated from individual platinum nanoparticles in solution. (a) Scheme showing the experimental approach by collecting a movie of the single rotating platinum nanocrystal in a 2D projection. (b) Electron microscopy density map obtained from the 3D reconstruction of particle 1. The orientation of the particle is aligned to expose  $\{111\}$  planes of the core domain. Three distinct crystal domains can be identified. (c) Electron microscopy density map obtained from the 3D reconstruction of particle 2. (d) 3D electron microscopy density map of particle 1 with alternative viewing angles. (e) 3D electron microscopy density map of particle 2 with alternative viewing angles. Panels d and e present the two particles from the same angles and directions with respect to the orientations in panels b and c. Abbreviations: GLC, graphene liquid cell; TEM, transmission electron microscopy. Figure adapted from Reference 92 with permission.

beam, they also showed the trapping of multiple nanoparticles in a liquid cell. Chen et al. (69) reported that nanoparticles can be attracted outside of the electron beam. The driving force for electron beam manipulation was attributed to electric charging effects, and it is a function of the particle-to-beam distance. Overall, the nature of nanoparticle–electron beam interaction needs to be further studied.

Whereas the electron beam tweezing of nanoparticles may bring useful applications, the study of nanoparticle diffusion and assembly using liquid cell TEM requires careful control of electron beam perturbation. In addition to reducing the electron beam dose, it is necessary to perform control experiments in which the electron beam is shut down periodically for comparison.

## 5. ELECTRIC BIASING IN A LIQUID CELL

### 5.1. Electrochemical Deposition

Electrochemical experiments can be carried out using a liquid cell by adding patterned electrodes inside the cell. A wide range of materials [i.e., gold (14, 134), titanium, platinum (135), carbon] can be used as the electrodes, although gold electrodes are most commonly reported. The design concept of an electrochemical liquid cell is similar to that in **Figure 2b** except that in most recent work, an extra container is not added as a reservoir and the electrode configuration varies. With an electrochemical liquid cell, the electrochemical deposition of metal can be studied in situ (see **Figure 8**). **Figure 8a** shows the electrodeposition of copper in a liquid cell (30, 31). Copper growth takes place on a polycrystalline gold electrode from an acidified copper sulfate

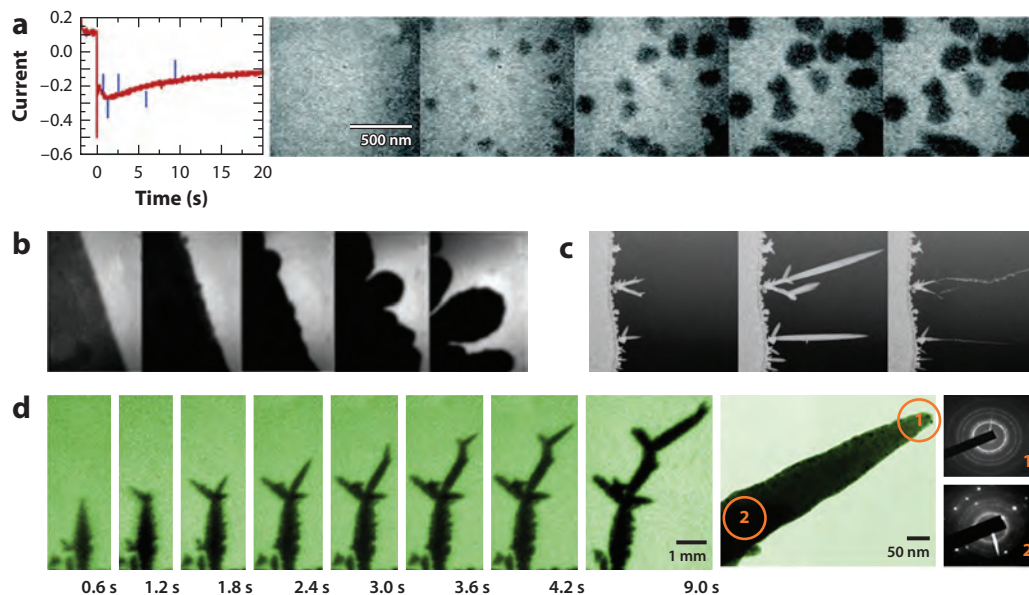


**Figure 8**

(a) Plot of current versus time recorded during the deposition of copper on polycrystalline gold at a potential of  $-0.07$  V. Panel *a* adapted from Reference 31 with permission. (b) Electrodeposition of copper onto polycrystalline platinum from the electrolyte in panel *a*. Panel *b* adapted from Reference 135 with permission. (c) Dendrite growth and collapse in  $1.5$  M  $\text{Pb}(\text{NO}_3)_2$  during application of square wave voltage pulses. Panel *c* adapted from Reference 19 with permission. (d) Sequential transmission electron microscopy images showing the electrochemical growth of lead dendrites. Panel *d* adapted from Reference 134 with permission.

electrolyte under an electric bias with constant voltage. The spatial distribution and growth kinetics of individual copper islands can be captured. The growth of copper clusters can be correlated with the applied electrochemical program. Pathways of copper diffusion and the island nucleation and growth mechanisms can be explored by comparing the growth rates measured from video of in situ experiments with that calculated from electrochemical models. Furthermore, scaling the island volumes and hence charge passed from the imaged area ( $2 \text{ } \mu\text{m}^2$ ) to the total electrode area ( $2,000 \text{ } \mu\text{m}^2$ ), and comparing with the measured current, suggests that all areas of the electrode are behaving uniformly, even those out of view. This type of calibration is important for the quantitative analysis of electrochemical processes.


Similar experiments examine the effects of additives and also of the electron beam (85). Instability occurs when the process is controlled by diffusion through the electrolyte so that areas projected further into the electrolyte can collect more ions and grow further. **Figure 8b** shows the development of an unstable copper growth front. The lateral growth of a uniform film can be achieved by controlling the growth and electrolyte chemistry. The lateral growth scenario provides an interesting model for the charging process in secondary batteries, such as those of zinc or lead batteries. In batteries, controlling growth front planarity is important, given that nonuniform deposition of metal onto the anode during charging can short the battery and cause damage or even a fire.

White et al. (19) reported lead electrodeposition in an electrochemical liquid cell (**Figure 8c**). With the applied electric potential program varied, lead dendrites either grew or were suppressed, with the results relevant to conventional lead-acid batteries. Sun et al. (134) investigated the growth mechanisms of lead dendrites as deposited on electrodes under an applied potential. They developed an electrochemical liquid cell by limiting the areas of electrode exposure to the electrolyte so that the observation under TEM represented the main stream of reaction inside the liquid cell and also avoided the possible issue of electrolyte completion in such nanodevices. The experiment provided detailed information on the development of lead dendrites by fast protrusion and tip splitting. With more in-depth characterization, the authors concluded that the tip of a branch comprises polycrystalline nanograins, which eventually develop into a single crystalline branch (**Figure 8d**). This study demonstrated the unique electrochemical growth of single crystal dendrites through nucleation, aggregation, alignment, and attachment of randomly oriented small grains. Additionally, it found that the lead concentration in the electrolyte drastically influences the morphology of dendritic formation.

## 5.2. Lithiation and Delithiation in a Liquid Cell Nanobattery

Tremendous progress has been made toward the direct observation of the structural and chemical evolution of electrodes for lithium ion batteries (LIBs). The first in situ TEM observation of the charge and discharge of LIBs was achieved with an open cell configuration by Wang et al. (99) and Huang et al. (100). The battery comprises a vacuum-compatible ionic liquid-based electrolyte, a single nanowire electrode, and bulk  $\text{LiCoO}_2$  as the counter electrode. A typical ionic liquid electrolyte consists of 10% lithium bis(trifluoromethane sulfonyl)imide ( $\text{LiTFSI}$ ) dissolved in a hydrophobic ionic liquid, 1-butyl-1-methylpyrrolidinium ( $\text{P}_{14}$ ) TFSI ( $\text{P}_{14}\text{TFSI}$ ). Wetting of the ionic liquid forms a thin layer of electrolyte around the nanowire. Therefore, this configuration to some extent mimics a real battery configuration, in that the liquid electrolyte forms a conformal coating around the active component in the electrode. The open cell configuration offers the possibility of atomic-level spatial resolution and the analytical capability to study the mechanisms of lithium ion insertion into electrode materials during the charge/discharge cycle (**Supplemental Figure 4**).

This open cell technique has helped reveal details of lithiation mechanisms and structural evolution in a range of materials, especially anode materials such as silicon (136), germanium

 Supplemental Material

(137),  $\text{Al}_2\text{O}_3$  (138),  $\text{SnO}_2$  (100),  $\text{ZnO}$  (139), graphene (140), and carbon nanotubes (141). This method does have its drawbacks. First, the electrolyte is only in point contact with the electrode. This presumably modifies the diffusion pattern of lithium ions in the electrode, so the results are not necessarily representative of the real battery for which the electrode is fully immersed in the liquid electrolyte. Second, the open cell configuration forbids the use of carbon-based volatile electrolytes in commercial LIBs. Finally, the polymerization of the ionic liquid electrolyte occurs under the electron beam, and the cell can be cycled only a limited number of times, which cannot reveal the structural evolution of electrode materials in real batteries.

Using a sealed liquid cell, Gu et al. (20) studied the lithiation and delithiation of a silicon nanowire in a battery-relevant electrolyte, and similar devices have been demonstrated by other groups (20, 86, 87, 142, 143). The complex reactions occurring at the electrode-electrolyte interface lead to the formation of a passive layer, the solid electrolyte interphase (SEI), at the electrode surface (144). The SEI is fundamental to battery performance and lifetime because it controls the passivation, stability, and impedance of the electrode. The structure, chemistry, and evolution of the SEI with the cycling of the battery are therefore of key interest for liquid cell electron microscopy studies. Two very recent reports used closed liquid cells to examine several aspects of SEI formation. During electrochemical lithiation and delithiation of gold anodes in an  $\text{LiPF}_6/\text{EC}/\text{DEC}$  electrolyte, Zheng et al. (142) found that lithiation occurs inhomogeneously, with lithium metal dendritic growth, electrolyte decomposition, and SEI formation during cyclic voltammetry (**Figure 9**). The SEI layer was observed to develop uniformly on one gold electrode, concurrently with lithium dendrite growth on the other electrode. Similarly, in another observation using  $\text{LiPF}_6/\text{EC}/\text{DMC}$  (87), SEI formed in a dendritic rather than a uniform layer on a gold electrode. The SEI formed prior to the deposition of lithium and remained on the surface after lithium dissolution. Dendritic SEI formation prior to lithium deposition suggests that the electrolyte composition affects lithium deposition. Lithium deposition was also observed by other groups (94, 145), and the lithium-gold reaction was studied by Zeng et al. (84) in a commercial electrolyte.

Lithium ion transport in  $\text{LiFePO}_4 \leftrightarrow \text{FePO}_4$  serves as the prototypical example to address scientific questions related to ionic transport in cathode materials. It is known that removal and insertion of lithium ions in this system lead to a reversible phase transformation,  $\text{LiFePO}_4 \leftrightarrow \text{FePO}_4$ . Three models have been proposed to describe lithium ion transport: the shrinking-core (146), phase boundary migration (147), and solid solution (148) models. A systematic, quantitative understanding of the correlation of ionic transport with structure has yet to be established. With a closed liquid cell configuration, Holtz et al. (86) studied lithium ion transport kinetics and degradation mechanisms in  $\text{LiFePO}_4$  particles during charge/discharge cycles using energy-filtered TEM imaging. A valence energy loss peak at 5 eV was selected, which is unique for  $\text{FePO}_4$  but not for  $\text{LiFePO}_4$ . This allows the determination of the lithiation state of an  $\text{LiFePO}_4$  electrode and the surrounding aqueous electrolyte in real time with nanoscale resolution during electrochemical charge and discharge. Delithiation occurs particle by particle, with a slow nucleation and growth process within each particle starting at the edge and moving through the particle. The instantaneous enrichment/depletion of lithium captured during delithiation and lithiation of the particle highlights the advantages of nanoscale imaging under operando conditions.

## 6. BIOSCIENCE APPLICATIONS OF LIQUID CELL TRANSMISSION ELECTRON MICROSCOPY

Understanding cellular function at the molecular level requires techniques capable of imaging whole cells with a resolution that can image individual proteins in their native environment. Light microscopy has been used to image protein distributions via fluorescent labels in live cells in

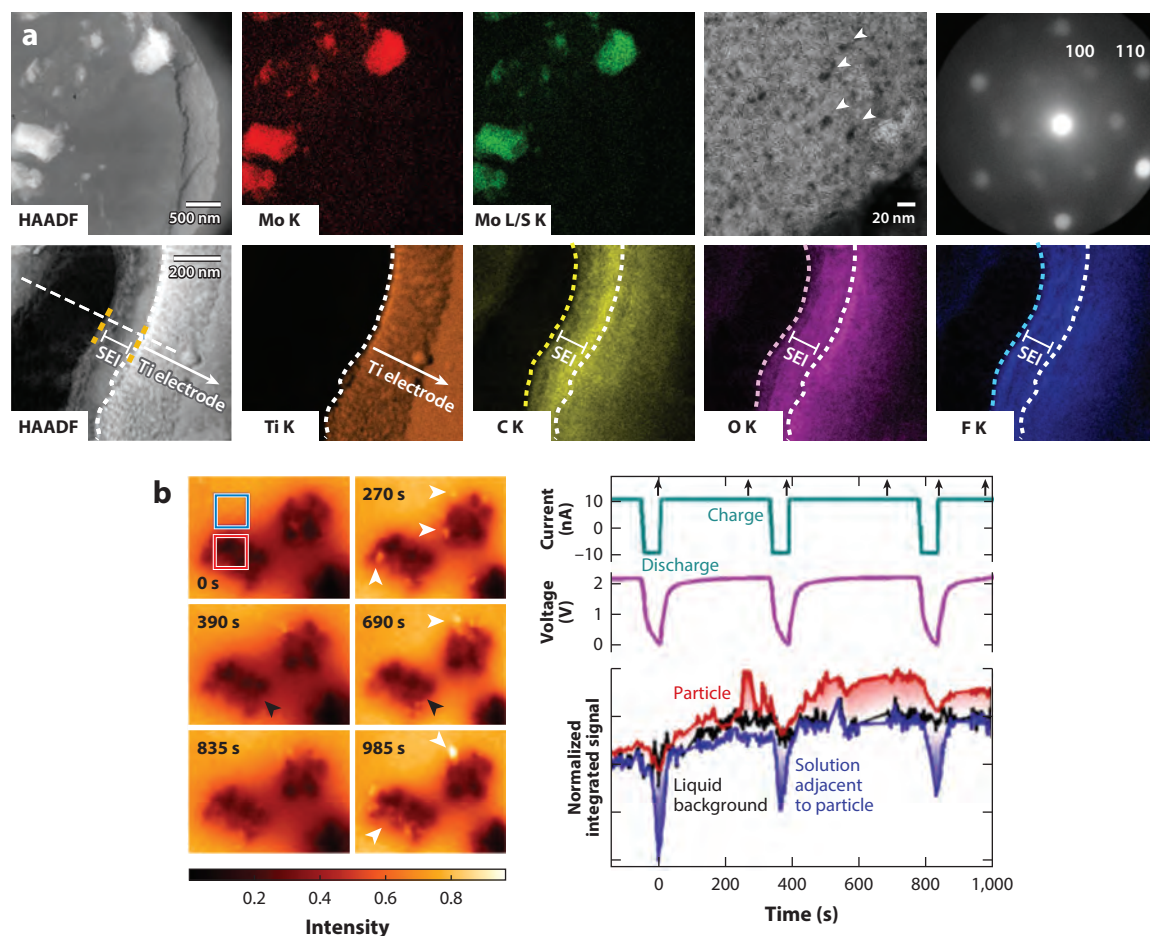


**Figure 9**

(a) In situ TEM observation of the MoS<sub>2</sub> reaction on a titanium electrode by using the electrochemical liquid cell and real-time electrode-electrolyte-interface formation in commercial LiPF<sub>6</sub>/EC/DEC electrolyte loaded in the liquid cell. Panel *a* adapted from Reference 93 with permission. (b, left) In situ energy-filtered TEM capturing the structural and chemical evolution of LiFePO<sub>4</sub> as a cathode and activated carbon counter electrode for a lithium ion battery. Regions of the particle are seen to light up and disappear, potentially owing to delithiating and fracturing off of the particle cluster. White arrowheads indicate bright charged particles and black arrowheads indicate dark discharged particles. (b, right) Integrated intensity over various regions, tracking with the voltage profile, from the regions shown at left by the boxes in red and blue. Panel *b* adapted from Reference 86 with permission. Abbreviations: SEI, solid electrolyte interphase; TEM, transmission electron microscopy.

liquid to investigate cellular function. Super-resolution techniques surpass the diffraction limit in optical microscopy but are still restricted to spatial resolutions of 10–20 nm. Electron microscopy is traditionally used to resolve the structures of individual proteins and to image protein distributions in cells. However, it demands sample preparation, such as protein crystals, stained thin sections, or frozen samples. The cells are thus not in their native liquid state. With the development of a liquid cell, it is possible to image cells and other biomaterials in their native environments. De Jonge and colleagues (34, 35) imaged cells in liquid with TEM by using a flow cell. The cells were placed in buffer solution in a liquid cell, and a spatial resolution of 4 nm and a pixel dwell

time of 20 ms were obtained. Huang et al. (43) described a self-aligned wet cell suitable for direct cell or bacteria incubation and observation in a wet environment inside a transmission electron microscope. Mirsaidov et al. (28) imaged acrosomal bundles in water in a self-contained liquid cell and determined the resolution to be at least 2.7 nm at doses of  $\sim 35 \text{ e}/\text{\AA}^2$ . (**Figure 10**). This

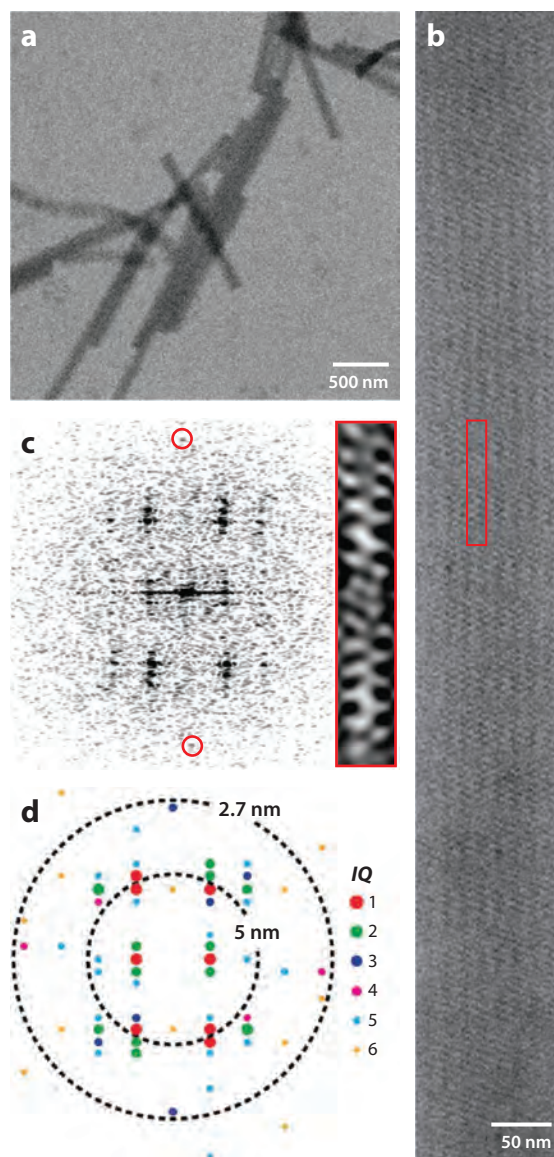



**Figure 10**

Imaging proteins in a liquid cell. (a) Low-magnification image of 80-nm-diameter acrosomal bundles in liquid. (b) An acrosomal bundle in h0l orientation. The unit cell is boxed in red. (c) Fourier transform pattern from a portion of the image of the acrosomal bundle in panel b. The meridional reflection at 2.7 nm is circled. The red box shows the unit cell reconstructed from reflections with a signal-to-noise ratio of  $>1.2$ . (d) IQ plot of the Fourier transform and the resolution shells at 5 and 2.7 nm. Figure adapted from Reference 28 with permission.

technique extends imaging of unstained and unlabeled macromolecular assemblies in water from the resolution of the light microscope to the nanometer resolution of the electron microscope.

Wang et al. (80) applied graphene liquid cells to other biological samples and examined them in their native state using aberration-corrected STEM. Atomic and electronic structures of hydrated ferritin were characterized using electron microscopy and spectroscopy through encapsulation in single-layer graphene in a biocompatible manner. It was demonstrated that graphene reduced the radiation damage to hydrogen bond breakage. The authors measured a reduction of the iron valence from 3+ to 2+ at nanometer resolution in ferritin, showing the initial stages of iron release by ferritin.

Park et al. (89) studied wet biological samples in a graphene liquid cell. The multilayer graphene sheets encapsulated and preserved biological samples in a liquid for TEM observation. They achieved nanometer-scale spatial resolution with high contrast using low-dose TEM at room temperature and used the graphene liquid cell to directly observe the structure of influenza viruses in their native buffer solution at room temperature. The graphene liquid cell was further extended to investigate whole cells in wet conditions with TEM (**Supplemental Figure 5**).

 **Supplemental Material**

## 7. ROLE OF THE ELECTRON BEAM AND ELECTRON BEAM DAMAGE CONTROL

In an in situ TEM experiment, one needs to understand how the imaging electrons modify the sample before drawing any conclusions about the mechanism of the process under study. For solid samples, the effect of a high-energy electron beam has been studied in detail both theoretically and experimentally (30, 31, 78, 85). The mechanisms of electron beam damage for imaging liquid samples can be different from those for solids, such as metals and semiconductors, given that various radicals, including secondary electrons, can be generated and these species can further participate in the reactions, which make the mechanism of radiation damage more complicated and system dependent.

According to Grogan et al. (135), high-energy electrons generate primary and secondary radiolysis products. These products rapidly (within seconds) reach equilibrium concentrations in the region irradiated by the electron beam. In the radiolysis of pure water, one product is hydrogen gas, which can produce bubbles if its steady-state concentration is above the solubility limit. Another product is hydrogen ions; thus, the electron beam can change the pH of a solution under study, which can alter the stability of other species in solution. A third, highly reactive product is the hydrated (or solvated) electron. It is thought to be responsible for the reduction of metallic cations in aqueous salt solutions, leading to the phenomena observed in experiments that measure the beam-induced growth of metallic nanoparticles (149, 150) and beam effects during electrochemical deposition (135). In more complex, nonaqueous solutions, such as the electrolytes for LIBs, the solvated electrons and other radical species can interact chemically with the salt and solvent. Identification and quantification of different species are needed for future study.

When liquid cell TEM is used to study nanoparticle growth, the electron beam is often used as the energy source to trigger the reaction. The high-energy electron beam can induce the decomposition of the liquid or precursor. Nanoparticle growth under the electron beam often occurs above a certain dose threshold. Although the electron beam can initiate nanoparticle growth, it can also induce side reactions. For example, with a sufficiently high dose rate, gaseous products, such as bubbles, can be generated in an aqueous solution (78).

**Supplemental Figure 6** summarizes a possible reaction pathway of nanoparticle growth in a liquid cell under an electron beam. The nucleation and growth of nanoparticles start from the supersaturation in the solution. There are different ways to initiate nanoparticle formation, such as

heat, chemical reduction, radiation, and the electron beam. As reported in many previous studies, nanoparticle growth under an electron beam shares many similarities with those of flask synthesis. A liquid cell TEM study of nanoparticle growth under thermal heating has also been reported, in which a commercial heating sample stage and a liquid cell compatible to the sample stage were used (49, 62).

The electron beam can also be utilized in a liquid cell to create beam-induced patterning at the nanoscale. Den Heijer et al. (85) patterned metal clusters using electrochemical deposition under the electron beam. By operating an electrochemical cell in a transmission electron microscope, they deposited copper on gold under potentiostatic conditions. When chloride ions were added into the liquid precursor, nucleation occurred only in areas irradiated by the electron beam under a range of applied potentials. By scanning the beam, patterns of deposited copper were generated. The process is analogous to laser-induced plating, but the high-energy electron beam can provide finer patterns, which can be useful for certain applications. Chen et al. (151) fabricated SiC<sub>x</sub> nanodots and nanowires with sizes from 60 nm to approximately 2  $\mu$ m using liquid cell TEM.

In general, to minimize the electron beam damage, one can consider reducing the accelerating voltage or lowering the electron dose. Depending on the specific system and the role of various factors, such as solvated electrons, bond cleavage, and local heating, there are different strategies to limit electron beam damage. According to Grogan et al. (78), during interactions of high-energy electrons with water, radiolysis plays an important role, but heating is typically insignificant. However, more vigorous study of the mechanisms of electron beam damage is highly sought. As all electron beam effects are dose dependent, low-dose imaging can be an effective way to reduce electron beam damage in all system. Techniques developed for biological imaging in cryo-electron microscopy can be very helpful in the future of imaging liquid samples.

## 8. OUTLOOK

Liquid cell TEM provides unique capabilities for the study of materials transformations in liquids with high spatial and temporal resolution. It has provided tremendous opportunities to observe colloidal nanoparticle nucleation and growth and many other materials and materials processes in liquid environments, such as the self-assembly of nanomaterials, electrochemical processes relevant to batteries, and biological imaging. Publications on liquid cell TEM have increased rapidly in the past several years. However, given the short time development, there is still much room for improvement.

In the future, more effort is needed and breakthroughs are expected in liquid cell TEM. For example, although atomic-scale resolution imaging has been achieved by incorporating ultrathin silicon nitride membranes or graphene in a liquid cell, improving the spatial resolution in liquid cell TEM is necessary for many studies. So far, the study of electrochemical processes in a liquid cell has been limited to low-resolution imaging, partly constrained by electron beam damage. Along with other approaches to control the damage, a highly sensitive detector is crucial for future developments. Moreover, improving the temporal resolution is important to study the transformation dynamics of materials, such as molecular dynamics in liquids. With the newly developed fast direct electron detection camera, imaging with a frame rate of 1,600 frames per second has been achieved. However, ultrafast imaging and spectroscopy (i.e., in a picosecond or femtosecond regime) is needed to understand certain scientific problems, and this area is under active research. Additionally, more capabilities need to be incorporated into liquid cell TEM. For instance, integrated highly sensitive and fast chemical detection and mapping are desired to study many reactions. Finally, we need to advance the liquid cell design or liquid cell TEM setup. Liquids with high vapor pressure (i.e., water and other low-boiling point organic solvents) are hard

to handle because they can easily dry out during sample loading or vanish under the electron beam, creating challenges for experiments and limiting the application of liquid cell TEM techniques. In addition, liquid cells with a well-calibrated environment, precursor mixing, and a controlled applied stimulus, for example, are often required to study certain controlled reactions. Advancing the liquid cell apparatus is an ongoing task.

We envision that as the technology matures, liquid cell TEM will experience revolutionary growth in the near future. It can become possible to reveal single molecules or individual atoms in liquids during reactions. Liquid cells allowing the mixing of different liquids in situ, fast detection, and mapping of different chemical species, a controlled local environment, can be achieved. Liquid cell TEM will continue to impact and advance broad interest in materials science, chemistry, physics, and biology.

## DISCLOSURE STATEMENT

The authors are not aware of any affiliations, memberships, funding, or financial holdings that might be perceived as affecting the objectivity of this review.

## ACKNOWLEDGMENTS

The authors thank Xiaowei Zhang for help with editing the references. We also thank the DOE Early Career Research Program for funding support.

## LITERATURE CITED

- Haider M, Uhlemann S, Schwan E, Rose H, Kabius B, Urban K. 1998. Electron microscopy image enhanced. *Nature* 392:768–69
- Urban KW. 2009. Is science prepared for atomic-resolution electron microscopy? *Nat. Mater.* 8:260–62
- Muller DA. 2009. Structure and bonding at the atomic scale by scanning transmission electron microscopy. *Nat. Mater.* 8:263–70
- Marton L. 1934. La microscopie électronique des objets biologiques. *Acad. R. Belg. Bull. Cl. Sci.* 20:439–46
- Abrams IM, McBain JW. 1944. A closed cell for electron microscopy. *J. Appl. Phys.* 15:607–9
- Swift JA, Brown AC. 1970. Environmental cell for examination of wet biological specimens at atmospheric pressure by transmission scanning electron microscopy. *J. Phys. E* 3:924–26
- Butler EP. 1979. In situ experiments in the transmission electron microscope. *Rep. Prog. Phys.* 42:833–95
- Fullam EF. 1972. Closed wet cell for electron microscope. *Rev. Sci. Instrum.* 43:245–47
- Dupouy G, Perrier F, Durrieu L. 1962. Microscopie électronique—l'observation des objets en milieu gazeux—application à l'étude de la contamination dans le microscope électronique. *C. R.* 254:3786–91
- Allinson DL. 1970. Environmental cell for use in a high voltage electron microscope. In *Proc. 7th Int. Congr. Electron Microsc.*, Vol. 1, ed. P Favard, pp. 169–70. Paris: Soc. Fr. Microsc. Electron.
- Fukami A, Etoh T, Ishihara N, Katoh M, Fujiwara K. 1970. Pressurized specimen chamber for electron microscope. In *Proc. 7th Int. Congr. Electron Microsc.*, Vol. 1, ed. P Favard, pp. 171–72. Paris: Soc. Fr. Microsc. Electron.
- Harutyunyan AR, Chen GG, Paronyan TM, Pigos EM, Kuznetsov OA, et al. 2009. Preferential growth of single-walled carbon nanotubes with metallic conductivity. *Science* 326:116–20
- Kim BJ, Tersoff J, Kodambaka S, Reuter MC, Stach EA, Ross FM. 2008. Kinetics of individual nucleation events observed in nanoscale vapor-liquid-solid growth. *Science* 322:1070–73
- Zheng HM, Smith RK, Jun YW, Kisielowski C, Dahmen U, Alivisatos AP. 2009. Observation of single colloidal platinum nanocrystal growth trajectories. *Science* 324:1309–12
- Liao H-G, Cui LK, Whitlam S, Zheng HM. 2012. Real-time imaging of Pt<sub>3</sub>Fe nanorod growth in solution. *Science* 336:1011–14

16. Evans JE, Jungjohann KL, Browning ND, Arslan I. 2011. Controlled growth of nanoparticles from solution with in situ liquid transmission electron microscopy. *Nano Lett.* 11:2809–13
17. Zheng HM, Claridge SA, Minor AM, Alivisatos AP, Dahmen U. 2009. Nanocrystal diffusion in a liquid thin film observed by in situ transmission electron microscopy. *Nano Lett.* 9:2460–65
18. Williamson MJ, Tromp RM, Vereecken PM, Hull R, Ross FM. 2003. Dynamic microscopy of nanoscale cluster growth at the solid-liquid interface. *Nat. Mater.* 2:532–36
19. White ER, Singer SB, Augustyn V, Hubbard WA, Mecklenburg M, et al. 2012. In situ transmission electron microscopy of lead dendrites and lead ions in aqueous solution. *ACS Nano* 6:6308–17
20. Gu M, Parent LR, Mehdi BL, Unocic RR, McDowell MT, et al. 2013. Demonstration of an electrochemical liquid cell for operando transmission electron microscopy observation of the lithiation/delithiation behavior of Si nanowire battery anodes. *Nano Lett.* 13:6106–12
21. Chen X, Noh KW, Wen JG, Dillon SJ. 2012. In situ electrochemical wet cell transmission electron microscopy characterization of solid-liquid interactions between Ni and aqueous NiCl. *Acta Mater.* 60:192–98
22. Mirsaidov U, Ohl C-D, Matsudaira P. 2012. A direct observation of nanometer-size void dynamics in an ultra-thin water film. *Soft Matter* 8:7108
23. White ER, Mecklenburg M, Singer SB, Aloni S, Regan BC. 2011. Imaging nanobubbles in water with scanning transmission electron microscopy. *Appl. Phys. Express* 4:055201
24. Li D, Nielsen MH, Lee JR, Frandsen C, Banfield JF, De Yoreo JJ. 2012. Direction-specific interactions control crystal growth by oriented attachment. *Science* 336:1014–18
25. Huang TW, Liu SY, Chuang YJ, Hsieh HY, Tsai CY, et al. 2013. Dynamics of hydrogen nanobubbles in KLH protein solution studied with in situ wet-TEM. *Soft Matter* 9:8856–61
26. Proetto MT, Rush AM, Chien M-P, Abellan Baeza P, Patterson JP, et al. 2014. Dynamics of soft nanomaterials captured by transmission electron microscopy in liquid water. *J. Am. Chem. Soc.* 136:1162–65
27. de Jonge N, Peckys DB, Kremers GJ, Piston DW. 2009. Electron microscopy of whole cells in liquid with nanometer resolution. *PNAS* 106:2159–64
28. Mirsaidov UM, Zheng HM, Casana Y, Matsudaira P. 2012. Imaging protein structure in water at 2.7 nm resolution by transmission electron microscopy. *Biophys. J.* 102:L15–17
29. Evans JE, Jungjohann KL, Wong PCK, Chiu P-L, Dutrow GH, et al. 2012. Visualizing macromolecular complexes with in situ liquid scanning transmission electron microscopy. *Micron* 43:1085–90
30. Radisic A, Vereecken PM, Hannon JB, Season PC, Ross FM. 2006. Quantifying electrochemical nucleation and growth of nanoscale clusters using real-time kinetic data. *Nano Lett.* 6:238–42
31. Radisic A, Ross F, Searson P. 2006. In situ study of the growth kinetics of individual island electrodeposition of copper. *J. Phys. Chem. B* 110:7862–68
32. Liu K-L, Wu C-C, Huang Y-J, Peng H-L, Chang H-Y, et al. 2008. Novel microchip for in situ TEM imaging of living organisms and bio-reactions in aqueous conditions. *Lab Chip* 8:1915–21
33. Donev EU, Hastings JT. 2009. Electron-beam-induced deposition of platinum from a liquid precursor. *Nano Lett.* 9:2715–18
34. Peckys DB, Veith GM, Joy DC, de Jonge N. 2009. Nanoscale imaging of whole cells using a liquid enclosure and a scanning transmission electron microscope. *PLOS ONE* 4:e8214
35. de Jonge N, Poirier-Demers N, Demers H, Peckys DB, Drouin D. 2010. Nanometer-resolution electron microscopy through micrometers-thick water layers. *Ultramicroscopy* 110:1114–19
36. Grogan JM, Bau HH. 2010. The nanoaquarium: a platform for in situ transmission electron microscopy in liquid media. *J. Microelectromech. Syst.* 19:885–94
37. Ring EA, de Jonge N. 2010. Microfluidic system for transmission electron microscopy. *Microsc. Microanal.* 16:622–29
38. Peckys DB, Dukes MJ, Ring EA, Piston DW, de Jonge N. 2011. Imaging specific protein labels on eukaryotic cells in liquid with scanning transmission electron microscopy. *Microsc. Today* 19:16–20
39. Grogan JM, Rotkina L, Bau HH. 2011. In situ liquid-cell electron microscopy of colloid aggregation and growth dynamics. *Phys. Rev. E* 83:061405
40. Donev EU, Schardein G, Wright JC, Hastings JT. 2011. Substrate effects on the electron-beam-induced deposition of platinum from a liquid precursor. *Nanoscale* 3:2709–17

41. Klein KL, Anderson IM, de Jonge N. 2011. Transmission electron microscopy with a liquid flow cell. *J. Microsc.* 242:117–23
42. Suga M, Nishiyama H, Konyuba Y, Iwamatsu S, Watanabe Y, et al. 2011. The Atmospheric Scanning Electron Microscope with open sample space observes dynamic phenomena in liquid or gas. *Ultramicroscopy* 111:1650–58
43. Huang T-W, Liu S-Y, Chuang Y-J, Hsieh H-Y, Tsai C-Y, et al. 2012. Self-aligned wet-cell for hydrated microbiology observation in TEM. *Lab Chip* 12:340–47
44. Mirsaidov UM, Zheng H, Bhattacharya D, Casana Y, Matsudaira P. 2012. Direct observation of stick-slip movements of water nanodroplets induced by an electron beam. *PNAS* 109:7187–90
45. Liu Y, Chen X, Noh KW, Dillon SJ. 2012. Electron beam induced deposition of silicon nanostructures from a liquid phase precursor. *Nanotechnology* 23:385302
46. Woehl TJ, Evans JE, Arslan I, Ristenpart WD, Browning ND. 2012. Direct in situ determination of the mechanisms controlling nanoparticle nucleation and growth. *ACS Nano* 6:8599–610
47. Park J, Kodambaka S, Ross FM, Grogan JM, Bau HH. 2012. In situ liquid cell transmission electron microscopic observation of electron beam induced Au crystal growth in a solution. *Microsc. Microanal.* 18:1098–99
48. Park J, Zheng HM, Lee WC, Geissler PL, Rabani E, Alivisatos AP. 2012. Direct observation of nanoparticle superlattice formation by using liquid cell transmission electron microscopy. *ACS Nano* 6:2078–85
49. Xin HL, Zheng H. 2012. In situ observation of oscillatory growth of bismuth nanoparticles. *Nano Lett.* 12:1470–74
50. Chen X, Wen J. 2012. In situ wet-cell TEM observation of gold nanoparticle motion in an aqueous solution. *Nanoscale Res. Lett.* 7:598
51. Zheng H, Mirsaidov UM, Wang L-W, Matsudaira P. 2012. Electron beam manipulation of nanoparticles. *Nano Lett.* 12:5644–48
52. Ring EA, de Jonge N. 2012. Video-frequency scanning transmission electron microscopy of moving gold nanoparticles in liquid. *Micron* 43:1078–84
53. White ER, Mecklenburg M, Shevitski B, Singer SB, Regan BC. 2012. Charged nanoparticle dynamics in water induced by scanning transmission electron microscopy. *Langmuir* 28:3695–98
54. Jungjohann KL, Evans JE, Aguiar JA, Arslan I, Browning ND. 2012. Atomic-scale imaging and spectroscopy for in situ liquid scanning transmission electron microscopy. *Microsc. Microanal.* 18:621–27
55. Stoll JD, Kolmakov A. 2012. Electron transparent graphene windows for environmental scanning electron microscopy in liquids and dense gases. *Nanotechnology* 23:505704
56. Chen X, Zhou LH, Wang P, Zhao CJ, Miao XL. 2012. A study of nano materials and their reactions in liquid using in situ wet cell TEM technology. *Chin. J. Chem.* 30:2839–43
57. Welch DA, Faller R, Evans JE, Browning ND. 2013. Simulating realistic imaging conditions for in situ liquid microscopy. *Ultramicroscopy* 135:36–42
58. Kraus T, de Jonge N. 2013. Dendritic gold nanowire growth observed in liquid with transmission electron microscopy. *Langmuir* 29:8427–32
59. Liu YZ, Lin XM, Sun YG, Rajh T. 2013. In situ visualization of self-assembly of charged gold nanoparticles. *J. Am. Chem. Soc.* 135:3764–67
60. Liao H-G, Zheng HM. 2013. Liquid cell transmission electron microscopy study of platinum iron nanocrystal growth and shape evolution. *J. Am. Chem. Soc.* 135:5038–43
61. Liu Y, Tai K, Dillon SJ. 2013. Growth kinetics and morphological evolution of ZnO precipitated from solution. *Chem. Mater.* 25:2927–33
62. Niu K-Y, Park J, Zheng H, Alivisatos AP. 2013. Revealing bismuth oxide hollow nanoparticle formation by the Kirkendall effect. *Nano Lett.* 13:5715–19
63. Chen Q, Smith JM, Park J, Kim K, Ho D, et al. 2013. 3D motion of DNA-Au nanoconjugates in graphene liquid cell electron microscopy. *Nano Lett.* 13:4556–61
64. Holtz ME, Yu Y, Gao J, Abruna HD, Muller DA. 2013. In situ electron energy-loss spectroscopy in liquids. *Microsc. Microanal.* 19:1027–35
65. Jungjohann KL, Bliznakov S, Sutter PW, Stach EA, Sutter EA. 2013. In situ liquid cell electron microscopy of the solution growth of Au-Pd core-shell nanostructures. *Nano Lett.* 13:2964–70

66. Woehl TJ, Jungjohann KL, Evans JE, Arslan I, Ristenpart WD, Browning ND. 2013. Experimental procedures to mitigate electron beam induced artifacts during in situ fluid imaging of nanomaterials. *Ultramicroscopy* 127:53–63
67. Mueller C, Harb M, Dwyer JR, Miller RD. 2013. Nanofluidic cells with controlled pathlength and liquid flow for rapid, high-resolution in situ imaging with electrons. *J. Phys. Chem. Lett.* 4:2339–47
68. Liao H-G, Shao Y, Wang C, Lin Y, Jiang Y-X, Sun S-G. 2014. TEM study of fivefold twined gold nanocrystal formation mechanism. *Mater. Lett.* 116:299–303
69. Chen Y-T, Wang C-Y, Hong Y-J, Kang Y-T, Lai S-E, et al. 2014. Electron beam manipulation of gold nanoparticles external to the beam. *RSC Adv.* 4:31652–56
70. Liao HG, Cui LK, Whitelam S, Zhrebetskyy D, Xin HL, et al. 2014. Facet development during platinum nanocube growth. *Science* 345:916–19
71. Nielsen MH, Aloni S, De Yoreo JJ. 2014. In situ TEM imaging of  $\text{CaCO}_3$  nucleation reveals coexistence of direct and indirect pathways. *Science* 345:1158–62
72. De Clercq A, Dachraoui W, Margeat O, Pelzer K, Henry CR, Giorgio S. 2014. Growth of Pt-Pd nanoparticles studied in situ by HRTEM in a liquid cell. *J. Phys. Chem. Lett.* 5:2126–30
73. Sutter E, Jungjohann K, Bliznakov S, Courty A, Maisonhaute E, et al. 2014. In situ liquid-cell electron microscopy of silver-palladium galvanic replacement reactions on silver nanoparticles. *Nat. Commun.* 5:4946
74. Nielsen MH, Li D, Zhang H, Aloni S, Han TY, et al. 2014. Investigating processes of nanocrystal formation and transformation via liquid cell TEM. *Microsc. Microanal.* 20:425–36
75. Lewis EA, Haigh SJ, Slater TJA, He Z, Kulzick MA, et al. 2014. Real-time imaging and local elemental analysis of nanostructures in liquids. *Chem. Commun.* 50:10019–22
76. Niu K-Y, Liao H-G, Zheng H. 2014. Visualization of the coalescence of bismuth nanoparticles. *Microsc. Microanal.* 20:416–24
77. Bhattacharya D, Bosman M, Mokkapatil VR, Leong FY, Mirsaidov U. 2014. Nucleation dynamics of water nanodroplets. *Microsc. Microanal.* 20:407–15
78. Grogan JM, Schneider NM, Ross FM, Bau HH. 2014. Bubble and pattern formation in liquid induced by an electron beam. *Nano Lett.* 14:359–64
79. Chen Q, Smith JM, Rasool HI, Zettl A, Alivisatos AP. 2014. Studies of the dynamics of biological macromolecules using Au nanoparticle-DNA artificial molecules. *Faraday Discuss.* 175:203–14
80. Wang C, Qiao Q, Shokuhfar T, Klie RF. 2014. High-resolution electron microscopy and spectroscopy of ferritin in biocompatible graphene liquid cells and graphene sandwiches. *Adv. Mater.* 26:3410–14
81. Sutter EA, Sutter PW. 2014. Determination of redox reaction rates and orders by in situ liquid cell electron microscopy of Pd and Au solution growth. *J. Am. Chem. Soc.* 136:16865–70
82. Zhu G, Jiang Y, Lin F, Zhang H, Jin C, et al. 2014. In situ study of the growth of two-dimensional palladium dendritic nanostructures using liquid-cell electron microscopy. *Chem. Commun.* 50:9447–50
83. Buchkremer A, Linn MJ, Timper JU, Eckert T, Mayer J, et al. 2014. Synthesis and internal structure of finite-size DNA-gold nanoparticle assemblies. *J. Phys. Chem. C* 118:7174–84
84. Zeng Z, Liang W-I, Chu Y-H, Zheng H. 2015. In situ TEM study of the Li-Au reaction in an electrochemical liquid cell. *Faraday Discuss.* 176:95–107
85. den Heijer M, Shao I, Radisic A, Reuter MC, Ross FM. 2014. Patterned electrochemical deposition of copper using an electron beam. *APL Mater.* 2:022101
86. Holtz ME, Yu Y, Gunceler D, Gao J, Sundararaman R, et al. 2014. Nanoscale imaging of lithium ion distribution during in situ operation of battery electrode and electrolyte. *Nano Lett.* 14:1453–59
87. Sacci RL, Dudney NJ, More KL, Parent LR, Arslan I, et al. 2014. Direct visualization of initial SEI morphology and growth kinetics during lithium deposition by in situ electrochemical transmission electron microscopy. *Chem. Commun.* 50:2104–7
88. Niu K, Frolov T, Xin HL, Wang J, Asta M, Zheng H. 2015. Bubble nucleation and migration in a lead-iron hydr(oxide) core-shell nanoparticle. *PNAS* 112:12928–32
89. Park J, Park H, Ercius P, Pegoraro AF, Xu C, et al. 2015. Direct observation of wet biological samples by graphene liquid cell transmission electron microscopy. *Nano Lett.* 15:4737–44

90. Patterson JP, Abellan P, Denny MS Jr., Park C, Browning ND, et al. 2015. Observing the growth of metal-organic frameworks by in situ liquid cell transmission electron microscopy. *J. Am. Chem. Soc.* 137:7322–28
91. Shin D, Park JB, Kim Y-J, Kim SJ, Kang JH, et al. 2015. Growth dynamics and gas transport mechanism of nanobubbles in graphene liquid cells. *Nat. Commun.* 6:6068
92. Park J, Elmlund H, Ercius P, Yuk JM, Limmer DT, et al. 2015. Nanoparticle imaging. 3D structure of individual nanocrystals in solution by electron microscopy. *Science* 349:290–95
93. Zeng Z, Zhang X, Bustillo K, Niu K, Gammer C, et al. 2015. In situ study of lithiation and delithiation of MoS<sub>2</sub> nanosheets using electrochemical liquid cell transmission electron microscopy. *Nano Lett.* 15:5214–20
94. Mehdi BL, Qian J, Nasybulin E, Park C, Welch DA, et al. 2015. Observation and quantification of nanoscale processes in lithium batteries by operando electrochemical (S)TEM. *Nano Lett.* 15:2168–73
95. de Jonge N, Ross FM. 2011. Electron microscopy of specimens in liquid. *Nat. Nano* 6:695–704
96. Yuk JM, Park J, Ercius P, Kim K, Hellebusch DJ, et al. 2012. High-resolution EM of colloidal nanocrystal growth using graphene liquid cells. *Science* 336:61–64
97. Tai K, Liu Y, Dillon SJ. 2014. In situ cryogenic transmission electron microscopy for characterizing the evolution of solidifying water ice in colloidal systems. *Microsc. Microanal.* 20:330–37
98. Creemer JF, Helveg S, Hoveling GH, Ullmann S, Molenbroek AM, et al. 2008. Atomic-scale electron microscopy at ambient pressure. *Ultramicroscopy* 108:993–98
99. Wang CM, Xu W, Liu J, Choi DW, Arey B, et al. 2010. In situ transmission electron microscopy and spectroscopy studies of interfaces in Li ion batteries: challenges and opportunities. *J. Mater. Res.* 25:1541–47
100. Huang JY, Zhong L, Wang CM, Sullivan JP, Xu W, et al. 2010. In situ observation of the electrochemical lithiation of a single SnO<sub>2</sub> nanowire electrode. *Science* 330:1515–20
101. Becker J, Schubert O, Sonnichsen C. 2007. Gold nanoparticle growth monitored in situ using a novel fast optical single-particle spectroscopy method. *Nano Lett.* 7:1664–69
102. Sun Y, Ren Y. 2013. In situ synchrotron X-ray techniques for real-time probing of colloidal nanoparticle synthesis. *Part. Part. Syst. Charact.* 30:399–419
103. Steinfeldt N. 2012. In situ monitoring of Pt nanoparticle formation in ethylene glycol solution by SAXS-influence of the NaOH to Pt ratio. *Langmuir* 28:13072–79
104. Polte J, Erler R, Thünemann AF, Sokolov S, Ahner TT, et al. 2010. Nucleation and growth of gold nanoparticles studied via in situ small angle X-ray scattering at millisecond time resolution. *ACS Nano* 4:1076–82
105. Abecassis B, Testard F, Spalla O, Barboux P. 2007. Probing in situ the nucleation and growth of gold nanoparticles by small-angle X-ray scattering. *Nano Lett.* 7:1723–27
106. Miao J, Chen C-C, Song C, Nishino Y, Kohmura Y, et al. 2006. Three-dimensional GaN-Ga<sub>2</sub>O<sub>3</sub> core shell structure revealed by X-ray diffraction microscopy. *Phys. Rev. Lett.* 97:215503
107. Ramesh GV, Sreedhar B, Radhakrishnan TP. 2009. Real time monitoring of the in situ growth of silver nanoparticles in a polymer film under ambient conditions. *Phys. Chem. Chem. Phys.* 11:10059–63
108. Simm AO, Ji XB, Banks CE, Hyde ME, Compton RG. 2006. AFM studies of metal deposition: instantaneous nucleation and the growth of cobalt nanoparticles on boron-doped diamond electrodes. *ChemPhysChem* 7:704–9
109. Kolmakov A, Goodman DW. 2002. In situ scanning tunneling microscopy of oxide-supported metal clusters: nucleation, growth, and thermal evolution of individual particles. *Chem. Rec.* 2:446–57
110. Oezaslan M, Hasche F, Strasser P. 2011. In situ observation of bimetallic alloy nanoparticle formation and growth using high-temperature XRD. *Chem. Mater.* 23:2159–65
111. Aabdin Z, Lu J, Zhu X, Anand U, Loh ND, et al. 2014. Bonding pathways of gold nanocrystals in solution. *Nano Lett.* 14:6639–43
112. Woehl TJ, Park C, Evans JE, Arslan I, Ristenpart WD, Browning ND. 2013. Direct observation of aggregative nanoparticle growth: kinetic modeling of the size distribution and growth rate. *Nano Lett.* 14:373–78
113. Murphy CJ, San TK, Gole AM, Orendorff CJ, Gao JX, et al. 2005. Anisotropic metal nanoparticles: synthesis, assembly, and optical applications. *J. Phys. Chem. B* 109:13857–70

114. Daniel MC, Astruc D. 2004. Gold nanoparticles: assembly, supramolecular chemistry, quantum-size-related properties, and applications toward biology, catalysis, and nanotechnology. *Chem. Rev.* 104:293–346
115. Gibbs JW, Bumstead HA, Van Name RG, Longley WR. 1902. *The Collected Works of J. Willard Gibbs*. Madison, WI: Longmans, Green & Co.
116. Wulff G. 1901. On the question of speed of growth and dissolution of crystal surfaces. *Z. Kristallogr. Mineral.* 34:449–530
117. Xia Y, Xiong Y, Lim B, Skrabalak SE. 2009. Shape-controlled synthesis of metal nanocrystals: Simple chemistry meets complex physics? *Angew. Chem. Int. Ed.* 48:60–103
118. Tian N, Zhou Z-Y, Sun S-G, Ding Y, Wang ZL. 2007. Synthesis of tetrahedral platinum nanocrystals with high-index facets and high electro-oxidation activity. *Science* 316:732–35
119. Bealing CR, Baumgardner WJ, Choi JJ, Hanrath T, Hennig RG. 2012. Predicting nanocrystal shape through consideration of surface-ligand interactions. *ACS Nano* 6:2118–27
120. Ringe E, Van Duyn RP, Marks LD. 2011. Wulff construction for alloy nanoparticles. *Nano Lett.* 11:3399–403
121. Liao H-G, Niu K, Zheng H. 2013. Observation of growth of metal nanoparticles. *Chem. Commun.* 49:11720–27
122. Kimura Y, Niinomi H, Tsukamoto K, García-Ruiz JM. 2014. In situ live observation of nucleation and dissolution of sodium chlorate nanoparticles by transmission electron microscopy. *J. Am. Chem. Soc.* 136:1762–65
123. Wu J, Gao W, Wen J, Miller DJ, Lu P, et al. 2015. Growth of Au on Pt icosahedral nanoparticles revealed by low-dose in situ TEM. *Nano Lett.* 15:2711–15
124. Parent LR, Robinson DB, Woehl TJ, Ristenpart WD, Evans JE, et al. 2012. Direct in situ observation of nanoparticle synthesis in a liquid crystal surfactant template. *ACS Nano* 6:3589–96
125. Parent LR, Robinson DB, Cappillino PJ, Hartnett RJ, Abellan P, et al. 2014. In situ observation of directed nanoparticle aggregation during the synthesis of ordered nanoporous metal in soft templates. *Chem. Mater.* 26:1426–33
126. Jiang Y, Zhu G, Lin F, Zhang H, Jin C, et al. 2014. In situ study of oxidative etching of palladium nanocrystals by liquid cell electron microscopy. *Nano Lett.* 14:3761–65
127. Chee SW, Pratt SH, Hattar K, Duquette D, Ross FM, Hull R. 2014. Studying localized corrosion using liquid cell transmission electron microscopy. *Chem. Commun.* 51:168–71
128. Li F, Josephson DP, Stein A. 2011. Colloidal assembly: the road from particles to colloidal molecules and crystals. *Angew. Chem. Int. Ed.* 50:360–88
129. Baker JL, Widmer-Cooper A, Toney MF, Geissler PL, Alivisatos AP. 2009. Device-scale perpendicular alignment of colloidal nanorods. *Nano Lett.* 10:195–201
130. Oleshko VP, Howe JM. 2011. Are electron tweezers possible? *Ultramicroscopy* 111:1599–606
131. Batson PE, Reyes-Coronado A, Barrera RG, Rivacoba A, Echenique PM, Aizpurua J. 2012. Nanoparticle movement: plasmonic forces and physical constraints. *Ultramicroscopy* 123:50–58
132. Batson PE, Reyes-Coronado A, Barrera RG, Rivacoba A, Echenique PM, Aizpurua J. 2011. Plasmonic nanobilliards: controlling nanoparticle movement using forces induced by swift electrons. *Nano Lett.* 11:3388–93
133. Zheng H. 2013. Using molecular tweezers to move and image nanoparticles. *Nanoscale* 5:4070–78
134. Sun M, Liao H-G, Niu K, Zheng H. 2013. Structural and morphological evolution of lead dendrites during electrochemical migration. *Sci. Rep.* 3:3227
135. Grogan JM, Schneider NM, Ross FM, Bau HH. 2012. The nanoaquarium: a new paradigm in electron microscopy. *J. Indian Inst. Sci.* 92:295–308
136. Liu XH, Zheng H, Zhong L, Huang S, Karki K, et al. 2011. Anisotropic swelling and fracture of silicon nanowires during lithiation. *Nano Lett.* 11:3312–18
137. Liu XH, Huang S, Picraux ST, Li J, Zhu T, Huang JY. 2011. Reversible nanopore formation in Ge nanowires during lithiation-delithiation cycling: an in situ transmission electron microscopy study. *Nano Lett.* 11:3991–97

138. Liu Y, Hudak NS, Huber DL, Limmer SJ, Sullivan JP, Huang JY. 2011. In situ transmission electron microscopy observation of pulverization of aluminum nanowires and evolution of the thin surface  $\text{Al}_2\text{O}_3$  layers during lithiation-delithiation cycles. *Nano Lett.* 11:4188–94
139. Kushima A, Liu XH, Zhu G, Wang ZL, Huang JY, Li J. 2011. Leapfrog cracking and nanoamorphization of ZnO nanowires during in situ electrochemical lithiation. *Nano Lett.* 11:4535–41
140. Liu XH, Wang JW, Liu Y, Zheng H, Kushima A, et al. 2012. In situ transmission electron microscopy of electrochemical lithiation, delithiation and deformation of individual graphene nanoribbons. *Carbon* 50:3836–44
141. Liu Y, Zheng H, Liu XH, Huang S, Zhu T, et al. 2011. Lithiation-induced embrittlement of multiwalled carbon nanotubes. *ACS Nano* 5:7245–53
142. Zheng Z, Liang W-I, Liao H-G, Xin HL, Chu Y-H, Zheng H. 2014. Visualization of electrode–electrolyte interfaces in  $\text{LiPF}_6/\text{EC}/\text{DEC}$  electrolyte for lithium ion batteries via in situ TEM. *Nano Lett.* 14:1745–50
143. Unocic RR, Sacci RL, Brown GM, Veith GM, Dudney NJ, et al. 2014. Quantitative electrochemical measurements using in situ ec-S/TEM devices. *Microsc. Microanal.* 20:452–61
144. Xu K, von Cresce A, Lee U. 2010. Differentiating contributions to “ion transfer” barrier from interphasial resistance and  $\text{Li}^+$  desolvation at electrolyte/graphite interface. *Langmuir* 26:11538–43
145. Leenheer AJ, Jungjohann KL, Zavadil KR, Sullivan JP, Harris CT. 2015. Lithium electrodeposition dynamics in aprotic electrolyte observed in situ via transmission electron microscopy. *ACS Nano* 9:4379–89
146. Morgan D, Van der Ven A, Ceder G. 2004. Li conductivity in  $\text{Li}_x\text{MPO}_4$  ( $M = \text{Mn, Fe, Co, Ni}$ ) olivine materials. *Electrochem. Solid State Lett.* 7:A30–32
147. Gibot P, Casas-Cabanas M, Laffont L, Levasseur S, Carlach P, et al. 2008. Room-temperature single-phase Li insertion/extraction in nanoscale  $\text{Li}_x\text{FePO}_4$ . *Nat. Mater.* 7:741–47
148. Malik R, Zhou F, Ceder G. 2011. Kinetics of non-equilibrium lithium incorporation in  $\text{LiFePO}_4$ . *Nat. Mater.* 10:587–90
149. Belloni J. 2006. Nucleation, growth and properties of nanoclusters studied by radiation chemistry: application to catalysis. *Catal. Today* 113:141–56
150. Belloni J, Mostafavi M, Remita H, Marignier JL, Delcourt MO. 1998. Radiation-induced synthesis of mono- and multi-metallic clusters and nanocolloids. *N. J. Chem.* 22:1239–55
151. Chen X, Zhou L, Wang P, Cao H, Miao X, Wei F. 2014. A study of electron beam induced deposition and nano device fabrication using liquid cell TEM technology. *Chin. J. Chem.* 32:399–404



# Contents

The Independence of the Junior Scientist's Mind: At What Price? <i>Giacinto Scoles</i> .....	1
Vacuum Ultraviolet Photoionization of Complex Chemical Systems <i>Oleg Kostko, Biswajit Bandyopadhyay, and Musabid Ahmed</i> .....	19
Real-Time Probing of Electron Dynamics Using Attosecond Time-Resolved Spectroscopy <i>Krupa Ramasesha, Stephen R. Leone, and Daniel M. Neumark</i> .....	41
Charge-Carrier Dynamics in Organic-Inorganic Metal Halide Perovskites <i>Laura M. Herz</i> .....	65
Vibrational Control of Bimolecular Reactions with Methane by Mode, Bond, and Stereo Selectivity <i>Kopin Liu</i> .....	91
Interfacial Charge Transfer States in Condensed Phase Systems <i>Koen Vandewal</i> .....	113
Recent Advances in Quantum Dynamics of Bimolecular Reactions <i>Dong H. Zhang and Hua Guo</i> .....	135
Enhancing Important Fluctuations: Rare Events and Metadynamics from a Conceptual Viewpoint <i>Omar Valsson, Pratyush Tiwary, and Michele Parrinello</i> .....	159
Vibrational Heat Transport in Molecular Junctions <i>Dvira Segal and Bijay Kumar Agarwalla</i> .....	185
Gas-Phase Femtosecond Particle Spectroscopy: A Bottom-Up Approach to Nucleotide Dynamics <i>Vasilios G. Stavros and Jan R.R. Verlet</i> .....	211
Geochemical Insight from Nonlinear Optical Studies of Mineral-Water Interfaces <i>Paul A. Covert and Dennis K. Hore</i> .....	233

Charge Transfer Dynamics from Photoexcited Semiconductor Quantum Dots <i>Haiming Zhu, Ye Yang, Kaifeng Wu, and Tianquan Lian</i> .....	259
Valence Electronic Structure of Aqueous Solutions: Insights from Photoelectron Spectroscopy <i>Robert Seidel, Bernd Winter, and Stephen E. Bradforth</i> .....	283
Molecular Shape and the Hydrophobic Effect <i>Matthew B. Hillyer and Bruce C. Gibb</i> .....	307
Characterizing Localized Surface Plasmons Using Electron Energy-Loss Spectroscopy <i>Charles Cherqui, Niket Thakkar, Guoliang Li, Jon P. Camden, and David J. Masiello</i> .....	331
Computational Amide I 2D IR Spectroscopy as a Probe of Protein Structure and Dynamics <i>Mike Reppert and Andrei Tokmakoff</i> .....	359
Understanding the Surface Hopping View of Electronic Transitions and Decoherence <i>Joseph E. Subotnik, Amber Jain, Brian Landry, Andrew Petit, Wenjun Ouyang, and Nicole Bellonzi</i> .....	387
On the Nature of Bonding in Parallel Spins in Monovalent Metal Clusters <i>David Danovich and Sason Shaik</i> .....	419
Biophysical Insights from Temperature-Dependent Single-Molecule Förster Resonance Energy Transfer <i>Erik D. Holmstrom and David J. Nesbitt</i> .....	441
Next-Generation Force Fields from Symmetry-Adapted Perturbation Theory <i>Jesse G. McDaniel and J.R. Schmidt</i> .....	467
Measuring the Hydrodynamic Size of Nanoparticles Using Fluctuation Correlation Spectroscopy <i>Sergio Dominguez-Medina, Sishan Chen, Jan Blankenburg, Pattanawit Swanglap, Christy F. Landes, and Stephan Link</i> .....	489
Atomic and Molecular Collisions at Liquid Surfaces <i>Maria A. Tesa-Serrate, Eric J. Smoll Jr., Timothy K. Minton, and Kenneth G. McKendrick</i> .....	515
Theory of Linear and Nonlinear Surface-Enhanced Vibrational Spectroscopies <i>Dhabih V. Chulbai, Zhongwei Hu, Justin E. Moore, Xing Chen, and Lasse Jensen</i> ....	541

Single-Molecule Studies in Live Cells <i>Ji Yu</i> .....	565
Excited-State Properties of Molecular Solids from First Principles <i>Leeor Kronik and Jeffrey B. Neaton</i> .....	587
Water-Mediated Hydrophobic Interactions <i>Dor Ben-Amotz</i> .....	617
Semiclassical Path Integral Dynamics: Photosynthetic Energy Transfer with Realistic Environment Interactions <i>Mi Kyung Lee, Pengfei Huo, and David F. Coker</i> .....	639
Reaction Coordinates and Mechanistic Hypothesis Tests <i>Baron Peters</i> .....	669
Fundamental Properties of One-Dimensional Zinc Oxide Nanomaterials and Implementations in Various Detection Modes of Enhanced Biosensing <i>Jong-in Hahn</i> .....	691
Liquid Cell Transmission Electron Microscopy <i>Hong-Gang Liao and Haimei Zheng</i> .....	719

## Indexes

Cumulative Index of Contributing Authors, Volumes 63–67 .....	749
Cumulative Index of Article Titles, Volumes 63–67 .....	753

## Errata

An online log of corrections to *Annual Review of Physical Chemistry* articles may be found at <http://www.annualreviews.org/errata/physchem>